The Effects of Base Motion Variability and Soil Heterogeneity on Lateral Spreading of Mildly Sloping Ground

Mohamed A. ElGhoraiby[1*] and Majid T. Manzari [1]

Abstract

Centrifuge modeling has been used to observe some key characteristics of liquefiable soils during seismic motions. If carefully conducted, the results of centrifuge tests can be used for validation of constitutive models and numerical modeling tools. However, a thorough evaluation of numerical models requires knowledge of the soil properties and the uncertainties associated with these properties. Moreover, the base excitations achieved in centrifuge tests often vary from the target base excitation, and a fair evaluation of the quality of blind prediction of a centrifuge test requires an account of the uncertainties associated with the achieved base motion. This paper presents an analysis of the effects of the inherent variability present in the soil density and base motion on the lateral spreading of mildly sloping ground. The analysis combines fully-coupled non-linear finite element modeling with Monte Carlo simulation. The stochastic analysis is based on the variabilities observed in the density of the soil specimens and in the achieved base motions of the centrifuge tests conducted for the Liquefaction Experiments and Analysis Projects (LEAP): LEAP-GWU-2015 and LEAP-UCD-2017. The two-surface plasticity model for sand is used to model the soil response. The model is calibrated against element tests performed on Ottawa-F65 sand to determine its liquefaction strength. The finite element model is pre-validated through deterministic simulation of the centrifuge experiments conducted during the LEAP project. The sources of variability are identified and their magnitudes are quantified based on the results obtained from the LEAP centrifuge experiments. First, the effects of the soil spatial variability are presented. Then, the effects of the base motion variability are discussed. Finally the combined effects of the variability in the soil density and base motion are evaluated. The results obtained from the stochastic analysis are compared with the variability in the soil response observed in the centrifuge experiments. The results obtained from this study show that by carefully modeling the different sources of variability, the stochastic analysis was able to model the observed variability in the lateral displacement of the centrifuge experiments. The results obtained confirm the observation that the lateral displacement of liquefiable soil is more sensitive to the base excitation variability than the variability in the soil density.

1 Department of Civil and Environmental Engineering, George Washington University, Washington, DC, USA.

* Corresponding Author, ghoraiby@gwu.edu.

1. Introduction

Soil is a heterogeneous material that is variable in nature. This inherent variability influences the soil response to external loading. Therefore relying solely on the average measures of the soil properties in the analysis and design of geo-structural systems may not be a suitable approach. This is especially true as performance-based design is becoming more common within the geotechnical engineering practice. Accordingly, a stochastic analysis may be a more fitting methodology for analyzing the soil response to the high level of uncertainty present. In particular, utilizing the stochastic analysis in understanding the complex phenomena of soil liquefaction and its effects on civil infrastructure could lead to valuable insights.

The main objective of the work presented here is to evaluate the effects of unavoidable variations in the achieved soil density and base motions on the magnitudes of lateral spreading of mildly sloping soil specimens modeled in centrifuge. The analysis combines fully-coupled non-linear finite element modeling with the Monte Carlo simulation. The stochastic analysis is based on the variabilities observed in the Liquefaction Experiments and Analysis Projects (LEAP): LEAP-GWU-2015 and LEAP-UCD-2017 centrifuge experiments. In the following sections, first a brief review of current literature on the variability in soil properties, base motion variability and the applications of the stochastic analysis in geotechnical engineering is presented. Next, sources of variability in the soil density and base motion observed during the LEAP projects are discussed. Afterward, the consequences of these observed variabilities on the dynamic excess pore pressure generation and the magnitude of lateral spreading are presented. Finally, the variability in the results obtained from the stochastic analysis is compared to the variability observed in the experiments.

1.1. Soil Variability

The natural variability of soil has been studied by many researchers [1–5]. Lumb [1] evaluated the variability of various soil properties (Atterberg limits, compression index, the coefficient of consolidation, as well as the void ratio) in four typical natural soils. The probability distributions of these properties were shown to be estimated by a normal or log-normal distribution. Lacasse and Nadim [2] reported the probability distribution function as well as the mean and coefficient of variation for different soil properties. For the initial void ratio, a coefficient of variation ranging from 7 to 30 percent was reported. The reported values were obtained from data available in the literature and the sources of uncertainty were attributed to different soil types, stress conditions, test methods, stress history, codes of practice and testing errors or imprecisions, among many other factors. The variability in the soil properties stems from the uniqueness of the soil conditions in each situation. This results in high uncertainty leading to a coefficient of variation with different magnitudes that could be as high as 30%.

Variability has been categorized based on two aspects. The first is the source of the variability. In the source-based categorization, the variability is divided into epistemic and aleatory.

Epistemic variability pertains to the variability due to the lack of knowledge. This type of variability could be due to limited number of observations, uncertainty in the measurement, or assumed idealizations when modeling the natural phenomenon (model uncertainty) [6]. Aleatory variability (also known as inherent variability) describes the natural randomness of a variable. This type of variability cannot be reduced [6].

The second aspect based on which the variability is categorized is the nature of the variability. The variability could be described as spatial variability if the random variable is position dependent. Soil properties such as the density and permeability are examples of spatially variable random fields. This type of variability can be defined using two components. The first is a trend component and the second is a random component with zero-mean [2]. According to Vanmarcke [7], the fluctuation component is considered to be statistically homogeneous, with a constant mean and standard deviation and a correlation that depends on relative distance rather than absolute location. Several methods have been developed to measure the spatial correlation, e.g. Method of Moments, Maximum Likelihood, and Local Average Theory [8]. To model the spatial correlation, Vanmarcke [7] introduced the concept of correlation length which is a measure of the correlation function.

A survey of the correlation length for various soil properties is reported by DeGroot [9] and Lacasse and Nadim [2]. It is shown that the in-situ properties of soil such as the SPT and CPT have correlation lengths in the range of 15 to 30 meters horizontally and 1 to 3 meters vertically. It is also noted that the correlation length is influenced by the laboratory environment as the correlation length of laboratory undrained shear strength, S_u obtained from triaxial and direct simple shear tests is in the range of 0.3 to 0.6 m. This means that the correlation length is highly affected by the depositional method of the soil. Therefore, it is important in this study to consider the effects of the method used in the sample preparation of the centrifuge experiments on the correlation length of the achieved soil properties. The correlation length along with the mean and coefficient of variation provide an appropriate and more complete description of the spatially correlated random field. Therefore, in order to conduct a realistic stochastic analysis, these parameters should be carefully selected.

In addition to the spatial variability, another category of variability is the temporal variability. It describes how the random field changes with respect to time. A random variable that is constant with time is known as a stationary random variable, while a random variable that changes with time is known as a non-stationary random variable. The variability present in the base acceleration time history due to a seismic event is an example of a non-stationary random process. This is discussed further in the following section.

1.2. Base Motion Variability

While the variability in the soil affects the material properties and initial conditions, another source of variability stems from the variations in the applied base excitation. The causes of

variability in the base motion are various depending on the application. In the field, earthquakes are influenced by soil characteristics, fault type, and distance from the source, among others. In the laboratory, the target base motion is predetermined but the achieved base motions almost always vary with respect to the target motion. These variations are usually affected by the size of the experiment, stiffness of the containing box, the natural frequency of the centrifuge, the presence of damping, and many other factors. These sources of variability manifest themselves in the variations of the amplitude and the frequency content of the resulting base motion.

In order to provide seismic resistant design, engineers initially relied on estimates of intensity measures which describe the base motion in their seismic hazard analysis. Based on collected data of the past seismic activity, empirical relationships (attenuation relationships) are developed to provide estimates of intensity measures such as the peak ground acceleration (PGA), velocity (PGV) and displacement (PGD) as well as the response spectral acceleration (SA), velocity (SD) and displacement (SD) [10–12]. Attenuation relationships adopt a lognormal distribution for the intensity measures and provide an estimate of the mean and standard deviation [12]. While the statistics of the intensity measures can provide useful insight for the design of simple structures, it proves to be insufficient in the design of important structures such as nuclear power plants, dams, and bridges. For such structure, a nonlinear dynamic analysis is necessary [13].

The nonlinear dynamic analysis techniques are time-based methods which require a description of the base motion as a time history. These methods are feasible for deterministic analysis where the time history is known. However, in the case of modeling the variability in the base motion, these methods are proven to be more challenging. While it may be feasible to obtain estimates of intensity measures statistics, it is quite difficult to obtain the statistics of the full time-history. Unlike the variability of single parameters, the time history is a non-stationary random process where the mean and variance are functions of time. Hence, taking the direct average of a set of time histories would result in an average time history with intensity measures that differ from the average intensity measures of these time histories. Therefore, the response due to the direct average of the time histories is in turn different from the average response of these time histories.

Another way to look at the base motion is in the frequency domain. The Fourier transform and response spectrum are two methods used by engineers to describe a base motion in the frequency domain. The Fourier transform describes the frequency content of base motion, while the spectral response presents the natural frequency of the SDOF system responding to the base motion. Even though both Fourier transform and spectral response provide a representation of the base motion in the frequency domain, they are quite different. Unlike the Fourier transform, taking the average of the acceleration response spectral would produce intensity measures matching the average of the intensity measures. Hence the statistics of a sample of base motions is best described by the statistics of the response spectra.

While the description of the base motion statistics can be presented with the statistics of the response spectra, generating an artificial base motion to match the obtained statistics is

challenging. The reason is that the response spectrum method is not reversible, which means having a response spectrum of a base motion is insufficient to obtain a corresponding base motion. Different attempts were pursued to finding base motion corresponding to a target base motion.

One attempt is through a selection process where base motions are selected from a database to match a target design response spectra [14–18]. While this method may be useful for design purposes, it is not as useful for modeling the variability in a target base motion. Another method proposed by [19] focuses on utilizing the white noise for generating the random base motion. Gazetas et al. [19] attempted to model the effects of random vibrations on the response of dams. Two modifications were applied to a stationary white noise model (SWN) which has a constant power spectral density (PSD). The first is the use of the Tajimi-Kanai PSD function to model the frequency content of the target response spectrum. The second is the use of a build-up and decay function to model the rise and drop in the base motion.

A different approach has been adopted by other researchers which links the time history of the base motion to the spectral velocity and a power spectrum density (PSD) function [13,20–22]. The methods and approaches followed in the aforementioned literature propose an approximate solution for generating a base motion that is compatible with a target response spectrum. Due to the insufficiency of the response spectrum as a representation of the base motion, it may not be possible to obtain an exact and unique base motion solely from the response spectrum. Here an iterative approach inspired by the work of Preumont [21] was adopted to generate a synthetic time history. By decomposing a time history into a series of ramped sinusoidal motions with different amplitudes and frequencies, the iterative method used by Preumont [21] was utilized to adjust the amplitudes so the response spectrum of the synthetic motion would match the target.

1.3. Stochastic Analysis

As computational tools are advancing in efficiency and precision, numerical methods provide a more practical approach for studying the effects of soil variability. This is especially true since field data are scarce and limited while experimental data are expensive and time-consuming. As an analytical tool, the finite element method allows for the analysis of various geo-structural systems. Additionally, finite element method could be utilized in the stochastic analysis by coupling it with statistical methods.

There are currently two approaches that apply this concept. The first is known as the stochastic finite element method (SFEM). In SFEM the finite element method is combined with the truncated Taylor series [23–26]. The results obtained from the SFEM are estimates of the mean and variance of functions of the random variables analyzed. The second method is based on coupling the finite element method with Monte Carlo simulation. It is known as the random finite element method (RFEM) [27,28]. Similar to the SFEM, the RFEM allows for estimation of the mean and the variance of functions of the random variables analyzed. However, the RFEM allows for obtaining the time history of the random variables for each simulation event [29].

The influence of spatial variability on seismic-induced-liquefaction of soil has been studied by various researchers [30–36]. Popescu et al. [30,31] studied the seismically-induced settlement of liquefiable soils where the soil penetration resistance was treated as a random variable. The effects of soil variability were studied by modeling the free field response of liquefiable soils using both 2D and 3D finite element models. Montgomery and Boulanger [35] have recently presented a stochastic analysis on a multi-layer sloping ground composed of a liquefiable layer underlying a layer of non-liquefiable clay. The work of Popescu et al. [30,31] showed the influence of soil spatial variability on the dynamic excess pore pressures, while the work of Montgomery and Boulanger [35] focused on the settlement and lateral spreading in mildly sloping liquefiable grounds.

Lopez-Caballero and Modaressi-Farahmand-Razavi [37] studied the combined effects of base motion variability and soil spatial variability on the response of liquefiable soils. Synthetic base motions were generated for the MC simulations. Spatial variability of the soil was modeled based on the variability in shear modulus degradation, damping and liquefaction strength of the soil. The effects of different spatial correlation lengths on the variability of soil parameters and their consequences were considered. The study concluded that the soil response is more sensitive to base motion variability than spatial variability.

In the current, the effects of soil spatially variability and the variability of the base excitation will be first considered individually and then their combained effects will be presented and discussed.

2. LEAP Centrifuge Experiments

The Liquefaction Experiments and Analysis Project (LEAP) is a collaborative effort among several universities and research institutes across the world to investigate the liquefaction and its effects on geo-structures. The main objectives of LEAP are to generate an extensive database of centrifuge experiments which model the consequences of liquefaction on different geo-structures and to assess the capability of the current state-of-the-art constitutive/numerical modeling tools to predict the response of liquefiable soil. For the first two phases of the project (LEAP-GWU-2015 and LEAP-UCD-2017) the theme was lateral spreading of mildly sloping liquefiable ground.

Figures 1 and 2 show the schematics drawing of the centrifuge experiment model for the LEAP-GWU-2015 and LEAP-UCD-2017 projects. Kutter et al. [38,39] present a summary of the observations obtained from the experiments performed in these projects. The centrifuge specimen is composed of homogeneous Ottawa sand layer with a 5-degree slope. A rigid box is used as the container of the soil specimen. The height of the soil layer is 4 meter at the center, the length is 20 meters and the width is at least 9 meters in prototype scale.

The location of the accelerometers and pore pressure transducers are shown in Figures 1 and 2 and are specified at Tables 1 and 2. Three arrays of sensors are placed, at the center and at 3.5

meters away from the soil box walls. Required sensors are shown in bold, highly recommended sensors to be used in the centrifuge tests are shown in non-bold dashed lines, and recommended sensors are shown as non-bolded solid line symbols. The required sensors include AH11 and AH12 to measure the achieved base motion and are spaced consistently such that the yaw rotational acceleration can be determined. The vertical accelerometers, AV1 and AV2 are sensitive to container due to the rocking and Coriolis accelerations which depend on the shaking direction. The central vertical array (P1-P4 and AH1-AH4) were located to minimize the boundary effects from the rigid walls. The pore pressure transducers and accelerometers are offset 1.5 m in the transverse direction (section A-A) for constructability and reduction of sensor-to-sensor interaction. Additional surface markers were placed to determine the magnitude of lateral displacement.

The experiment was designed to be repeatable by all of the centrifuge facilities. Some centrifuge facilities have hydraulic shakers that produce 1-D horizontal shaking in the plane of spinning, while other facilities perform the shaking along the axis of the centrifuge. To account for the differences in orientation of the shaking direction in the radial acceleration field, the 5-degree slope in the shaking direction is to be superimposed on a curved surface corresponding to the centrifuge radius as shown in Figure 2. If the surface was not curved initially, it would become curved to some extent as a result of liquefaction; settlements associated with the forming of the curve would be superimposed on settlements due to consolidation and spreading down the 5-degree slope. The surface curvature is important to minimize differences between experiments at different facilities. Table 3 lists the properties of the participating centrifuge facilities including the model scale, shaking direction, centrifuge radius and the length to width ratio of the model container.

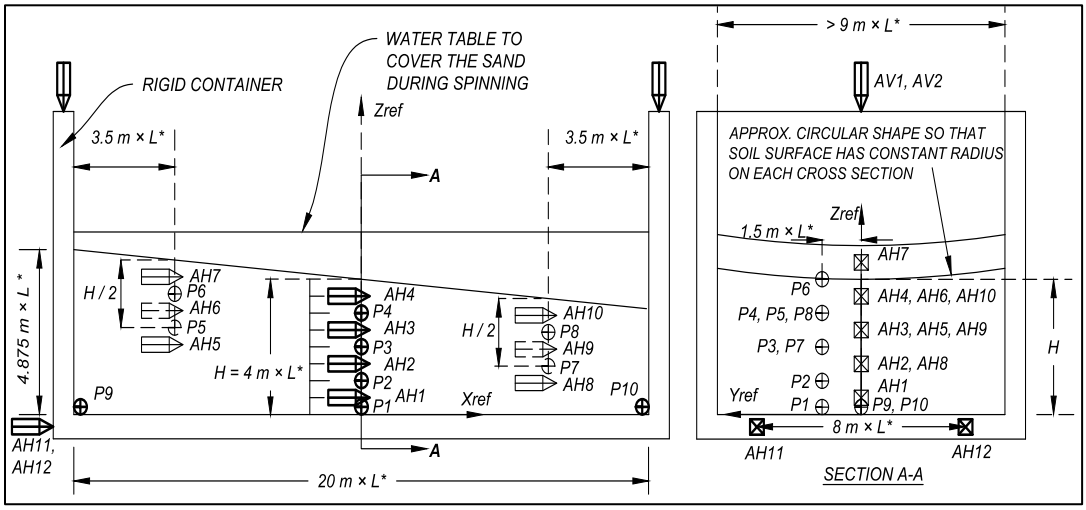

Figure 1: Baseline schematics of the LEAP Lateral Spreading Centrifuge Experiment for shaking parallel to the axis of rotation

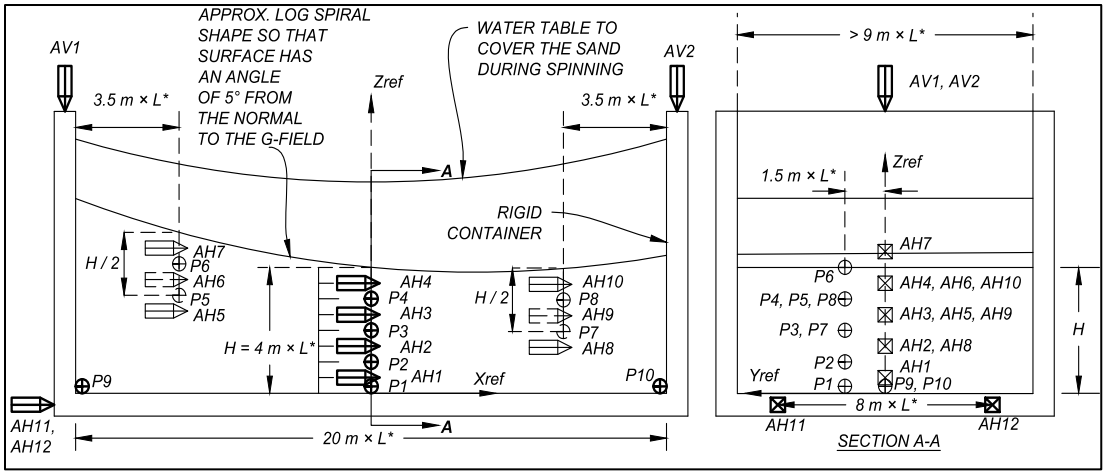

Figure 2: Baseline schematics and 3D rendering of the LEAP Lateral Spreading Centrifuge Experiment for shaking perpendicular to the axis of rotation

Table 1: Positions of the pore water pressure transducers of LEAP experiments

Sensor	P1	P2	P3	P4	P5	P6	P7	P8
x-pos. (m)	0.0	0.0	0.0	0.0	-6.5	-6.5	6.5	6.5
Depth (m)	4.0	3.0	2.0	1.0	2.0	1.0	2.0	1.0

Table 2: Positions of the accelerometers of LEAP experiments

Sensor	AH1	AH2	AH3	AH4	AH5	AH6	AH7	AH8	AH9	AH10
x-pos. (m)	0.0	0.0	0.0	0.0	-6.5	-6.5	-6.5	6.5	6.5	6.5
Depth (m)	3.5	2.5	1.5	0.5	2.5	1.5	0.5	2.5	1.5	0.5

Table 3: Centrifuge facilities participating in LEAP-UCD-2017, [39]

Facility	g*	Shaking direction	Radius of centrifuge (m)	Container Length/Width
CU	40.0	Tangential	4.125	0.45
KyU	44.4	Tangential	2.5	0.32
UCD	43.0	Tangential	1.0	0.63
NCU	26.0	Axial	3.0	0.45
RPI	23.0	Axial	3.0	0.42
ZJU	26.0	Axial	4.5	0.59
KAIST	40.0	Axial	5.0	0.45
IFSTTAR	50.0	Axial	5.06	0.50
Ehime	40.0	Axial	1.184	0.24

While the centrifuge experiments were carefully conducted unavoidable variabilities were present in the achieved base motion and soil density. Figure 7 compares the target void ratio and peak ground acceleration (PGA) with measured values in the LEAP-UCD-2017 centrifuge tests. The observed variability in the achieved soil properties was also reflected in the measurements of

the lateral spreading. Quantifying the contribution of these two random variables to the variability of the lateral spreading is the main goal here. More details on the experimental results obtained from the LEAP-GWU-2015 and LEAP-UCD-2017 could be obtained from the summary papers pertaining to these phases of the project by Kutter et al. [38,39].

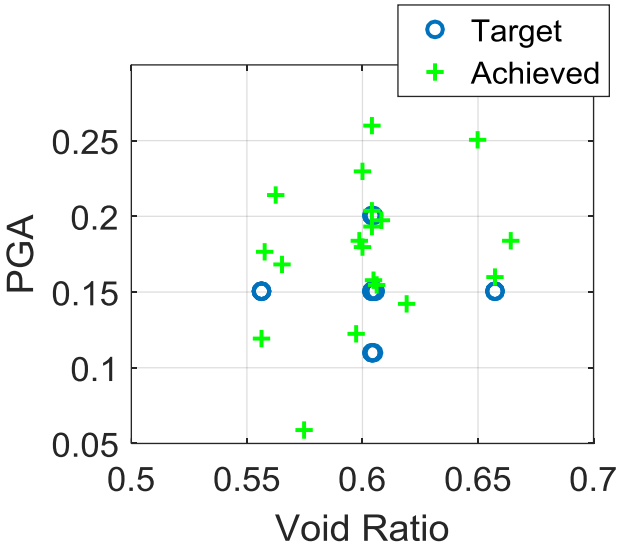

Figure 3: LEAP-UCD-2017 target test matrix and achieved experiments

3. Simulation of the LEAP Experiments

Before proceeding with the stochastic finite element analysis it is vital to calibrate, verify, and validate the constitutive and numerical modeling components of the analysis platform. Here, this is achieved by simulating the LEAP centrifuge experiments. First, the calibration process of the constitutive model is discussed. Afterwards, the finite element model is described. Finally, the simulation results are compared with the results of a set of centrifuge experiments that demonstrated consistency and repeatability.

3.1. Constitutive Model Calibration

The critical state two-surface plasticity model [40] is used to model the response of Ottawa F65 sand. The model was first introduced by Manzari and Dafalias [41] and then later revised in 2004 [40]. The model is based on the critical state soil mechanics framework by incorporating the state parameter in the formulations. This allows for the model to capture the soil response at different densities using a single set of model parameters. In the 2004 model (referred to here as MD04), a fabric tensor is introduced to account for the effect of fabric evolution during the dilatant phase of deformation on the subsequent contractant response of the soil upon load increment reversal. Additional details of the model formulation can be obtained in Dafalias and Manzari (2004).

The MD04 model has a total of 15 parameters that must be appropriately calibrated to capture the soil response in monotonic and cyclic loading conditions. Table 4 lists the model parameters which are grouped into five categories based on their functionality. In addition to conventional parameters such as Poisson's ratio, a few parameter may not appear to have a recognizable physical meaning, however, they are fundamental for the model definition. Calibration of these parameters is achieved by trial and error to obtain the base fit to the measured responses.

In this study, the model was calibrated by using a set of cyclic triaxial experiments which were performed by Vasko [42,43]. These experiments were provided to modelers in the LEAP-GWU-2015 prediction exercise [44]. The experiments are strain-controlled cyclic triaxial tests conducted on samples with a target density that matches the one for the centrifuge experiment of 1650 kg/m^3. The sample was prepared using dry pluviation with light tapping to reach the target density. The tests were done at confining stress of 200 kPa with cyclic strain amplitudes ranging from 0.05% to 0.4%. The main focus is to capture the liquefaction strength of the soil. Figure 4 shows a plot of the number of cycles it took for the soil to reach an excess pore pressure ratio, r_u, of 0.99 versus the cyclic strain amplitude. The simulated results are reasonably close to the experimentally obtained data points.

Table 4: MD04 calibrated model parameters for Ottawa F65 sand

Constant	Variable	Value
Elasticity	G_o	86
	ν	0.15
Critical state	M	1.27
	c	0.627
	λ_c	0.015
	e_o	0.745
	ξ	0.52
Yield surface	m	0.05
Plastic modulus	h_o	8.0
	c_h	0.498
	n^b	1.68
	A_o	0.49
	n^d	0.8
Fabric-dilatancy tensor	z_{max}	14
	c_z	3000

The calibrated model performance is further evaluated by simulating the element tests provided during the LEAP-UCD-2017 project [45–47]. The same data was used by modelers in the prediction exercise conducted as part of the project [48,49]. Figure 5 shows a comparison between the simulation and experiment in terms of the liquefaction strength. The element tests performed were stress-controlled cyclic triaxial tests on samples prepared with void ratio of 0.585 and confining stress of 100 kPa. It is observed that the calibrated model is able to capture the liquefaction strengths at higher CSRs but underestimates the liquefaction strength at smaller CSRs.

However this was considered to be satisfactory as majority of the centrifuge tests produce larger CSRs in the centrifuge soil specimen.

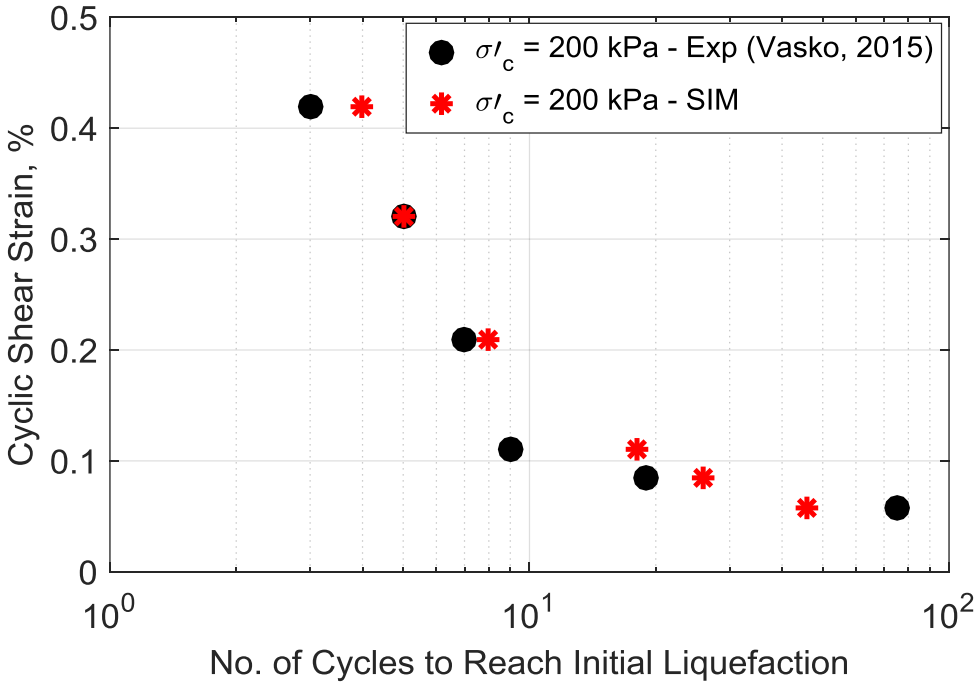

Figure 4: Comparison of the observed and simulated liquefaction strength curves for undrained strain-controlled cyclic triaxial tests on Ottawa F65 sand with confining stress of 200 kPa.

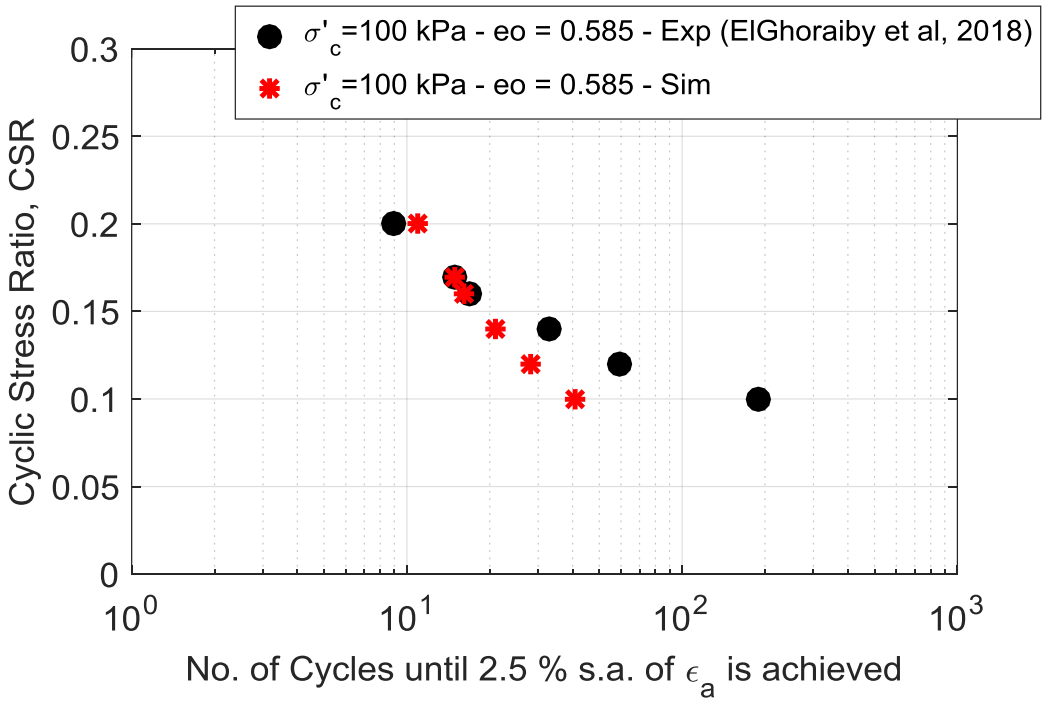

Figure 5: Comparison of the observed and simulated liquefaction strength curves for undrained stress-controlled cyclic triaxial tests on Ottawa F65 sand with confining stress of 100 kPa.

Once the calibrated model has satisfactorily simulated the element tests, the model was used in the simulation of the centrifuge experiments for further evaluation. Depending on how well the model performs additional recalibration may be necessary. In this case, the model results were compared to the centrifuge experiment performed at RPI during the LEAP-GWU-2015 project. As will be discussed in the following sections, the model was able to reasonably capture the excess pore pressure generation and the lateral displacements without any changes in the calibrated parameters. Hence, the model parameters shown in Table 4 were considered the finalized and were used for all of the simulations presented in the following sections.

3.2. Finite Element Model Description

The centrifuge experiment is modeled using the OpenSEES finite element platform (McKenna 1997). A convergence study is conducted where four different mesh densities are generated (Figure 6). The coarsest mesh is composed of 128 hydro-mechanically coupled four-node quadrilateral u-p elements. To increase the mesh density each element is subdivided into four elements. Therefore the remaining three meshes have the 512, 2048 and 8192 elements.

The boundary conditions of the models are highlighted in Figure 6. A fully fixed displacement boundary condition is assumed at the base. The nodes on the two sides of the model are fixed laterally while remaining free to move vertically. The nodes on the top surface are assumed to have complete free drainage. The simulations are composed of two stages. The first stage is known as the gravity stage, during which the state of stress due to gravitational (or centrifugal) acceleration is initialized. The second stage of the simulation is known as the dynamic stage, during this stage the model is subjected to the base motion.

The gravity stage is essential for obtaining accurate results during the dynamic stage. A steady state of stress must be achieved and correct initialization of the internal variables of the constitutive model must be reached before the dynamic step commences. For the simulations presented in this paper, the gravity stage was allowed to run for sufficient time to reach a steady state before proceeding with the dynamic analysis. Figure 7 shows the contour plots of the vertical, horizontal and shear stresses obtained from the analysis with the densest mesh, respectively.

The convergence of the simulation results is presented for the excess pore pressure as well as the displacement time histories. Figure 8 shows the excess pore pressure evolution during the earthquake at the location of the pore pressure transducer P1 shown in Figure 1. The results show that the rate of generation and the peak excess pore pressure do not change with the mesh density, while the dissipation rate slightly increases with the increase in the mesh density.

Figure 9 shows the plot of the lateral displacement and settlement time histories located near the top of the slope where the settlement is more significant. As the mesh density increased, it can be seen that the lateral displacement slightly increased while the soil settlement decreased. The percentage of the error between the different meshes as compared to the finest mesh is shown in Table 5. It can be seen from Table 5 that for the analysis using the mesh with 2048 elements the

error in x and y displacement became less than 1%. Hence this mesh used in the following numerical simulations.

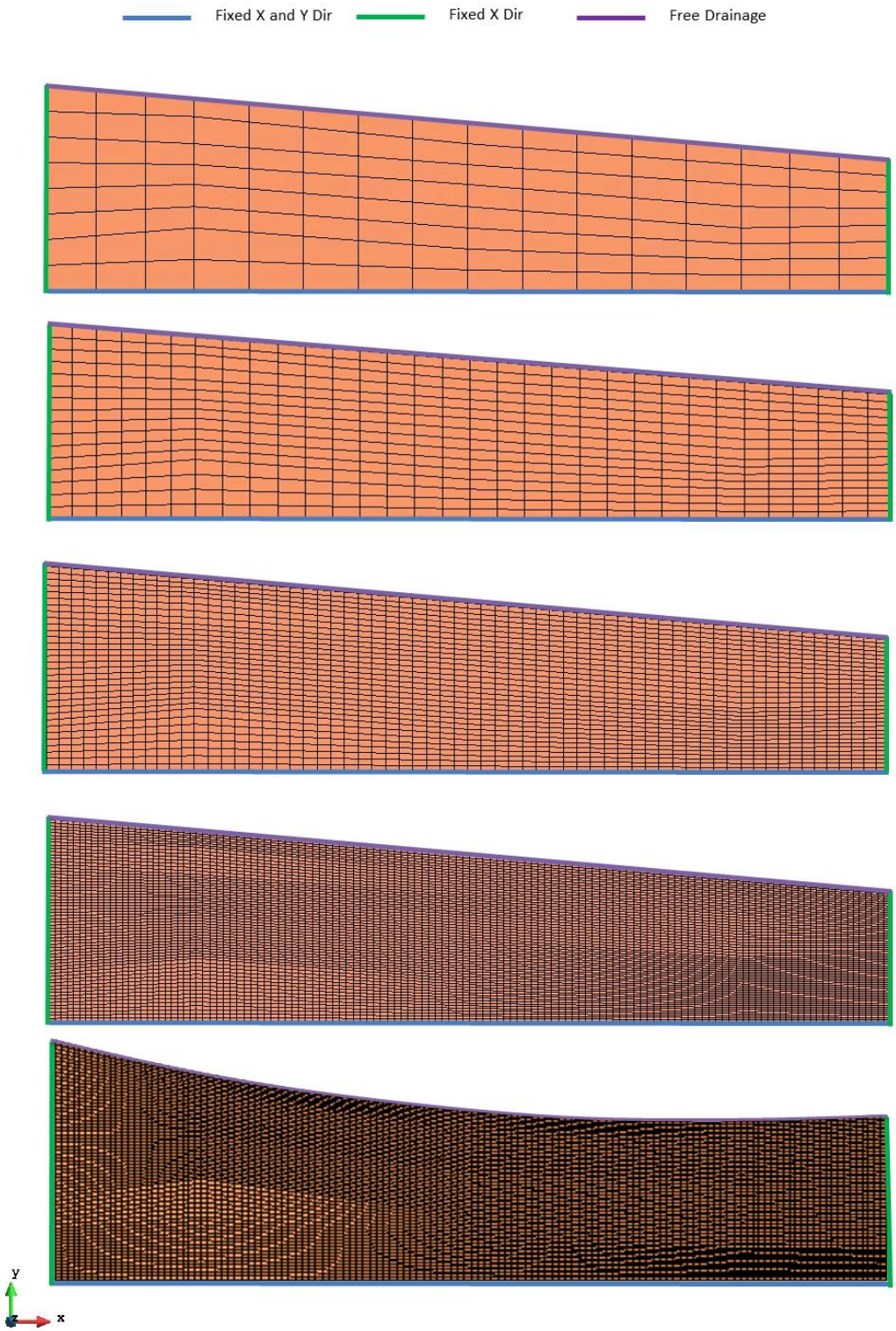

Figure 6: Finite Element Models: Coarse, Medium and Fine Mesh Densities

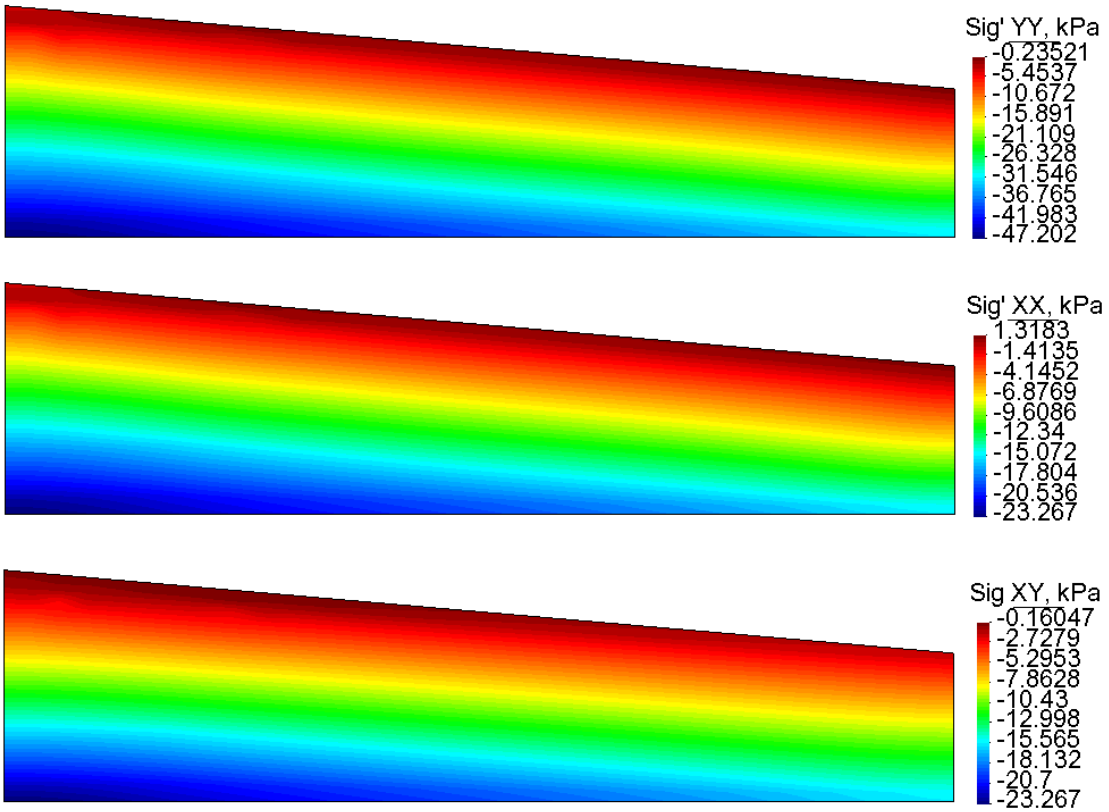

Figure 7: Initial state of stress at the end of the gravity stage

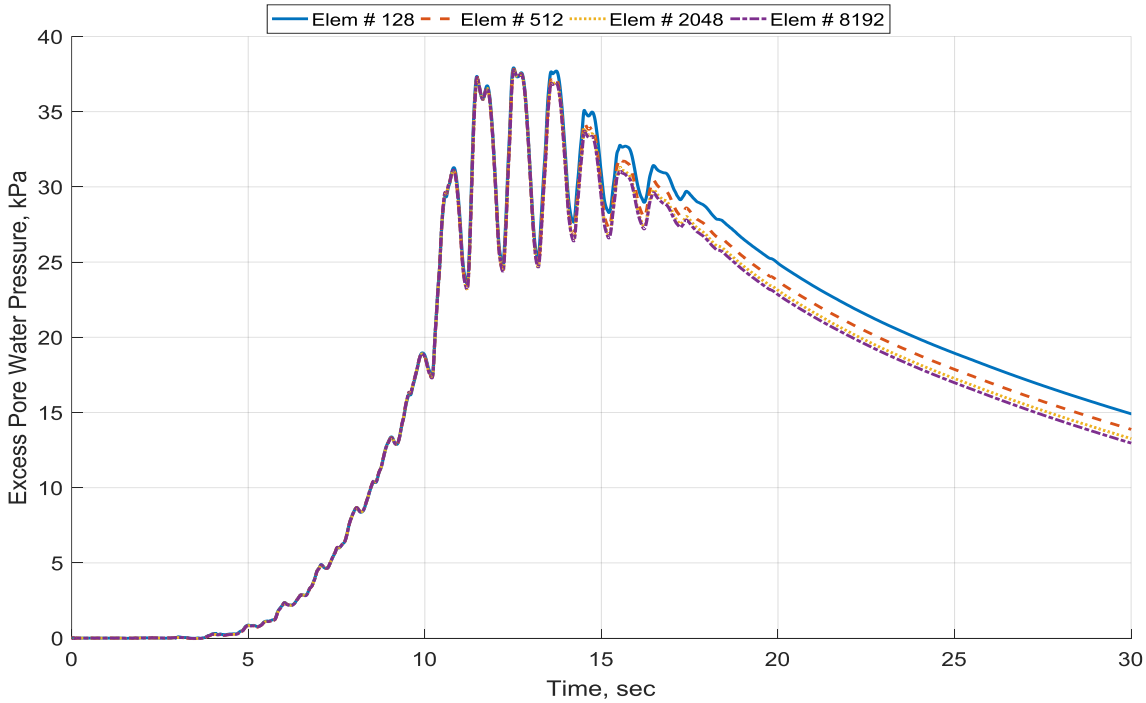

Figure 8: Convergence of the excess pore pressure at P1

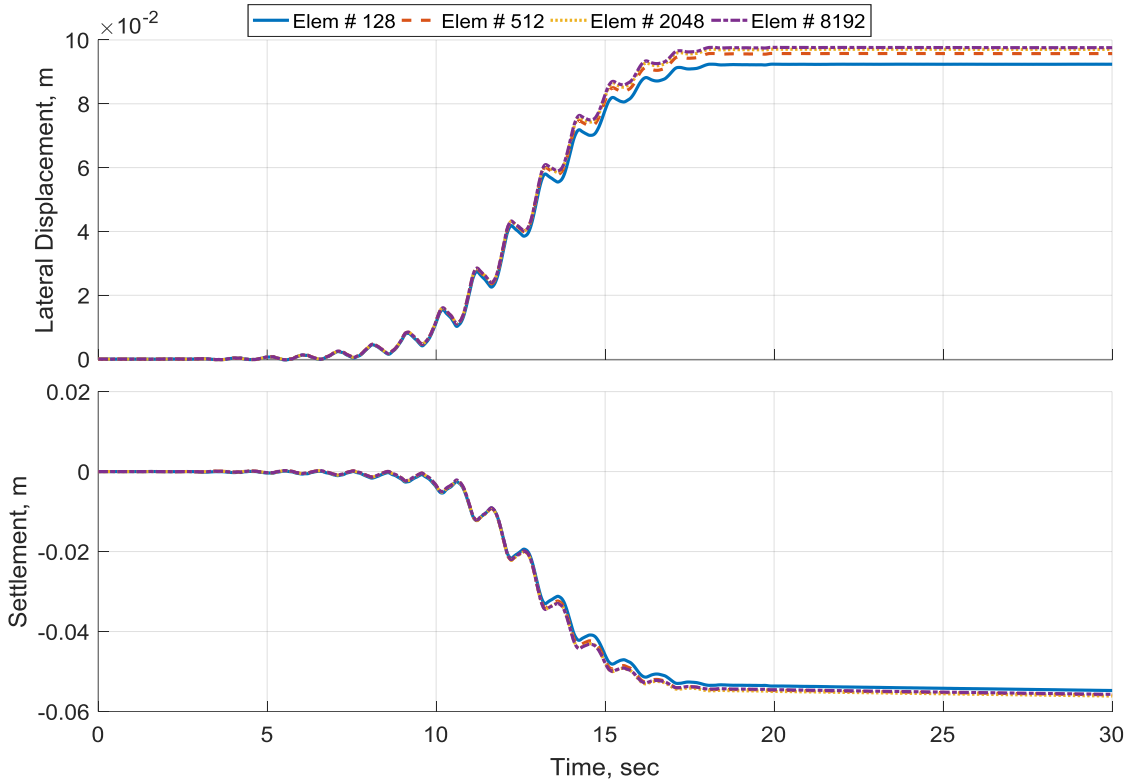

Figure 9: Convergence of the soil displacement at the top of the slope

Table 5: Displacement Errors

Constant	Error x (%)	Error y (%)
Elem # 128	5.624	3.076
Elem # 512	2.204	0.6465
Elem # 2048	0.722	0.337

3.3. Simulation Results of Selected Centrifuge Experiments

The Rensselaer Polytechnic Institute (RPI) participated in both LEAP-GWU-2015 and LEAP-UCD-2017 [50,51]. One of the RPI experiments performed during LEAP-UCD-2017 replicated the LEAP-GWU-2015 experiment. These two experiments showed consistency in the sample preparation as well as the achieved base motion as shown in Figure 10. For this reason, these two experiments are considered as benchmark experiments for evaluation of the model performance.

The RPI centrifuge applies the shaking in the direction parallel to the axis of rotation and therefore a flat surface model was adopted in all the RPI experiments. The soil was modeled with a 2048 element mesh (Figure 6).

3.3.1. Numerical Simulations of RPI15 and RPI17-1 Centrifuge Tests

Figure 10 shows the achieved base motions for RPI15 and RPI17-1 experiments [50,51]. It can be clearly seen that the input motion was successfully reproduced. The simulation results of these two experiments are presented herein.

First, the simulated excess pore water pressure time histories are compared with the experimental results. Figures 11 and 12 show the results of the excess pore water pressure time histories at the central sensor array for RPI15 and RPI17-1 experiments, respectively. The experimental results are shown in the top plot while the simulation results in the bottom plot. Reasonably good agreements are observed between the simulations and experiments in terms of the maximum excess pore pressure generated. Also, the model was able to predict reasonably well both the rate of generation and rate of dissipation of the excess pore pressure across the depth of the soil layer.

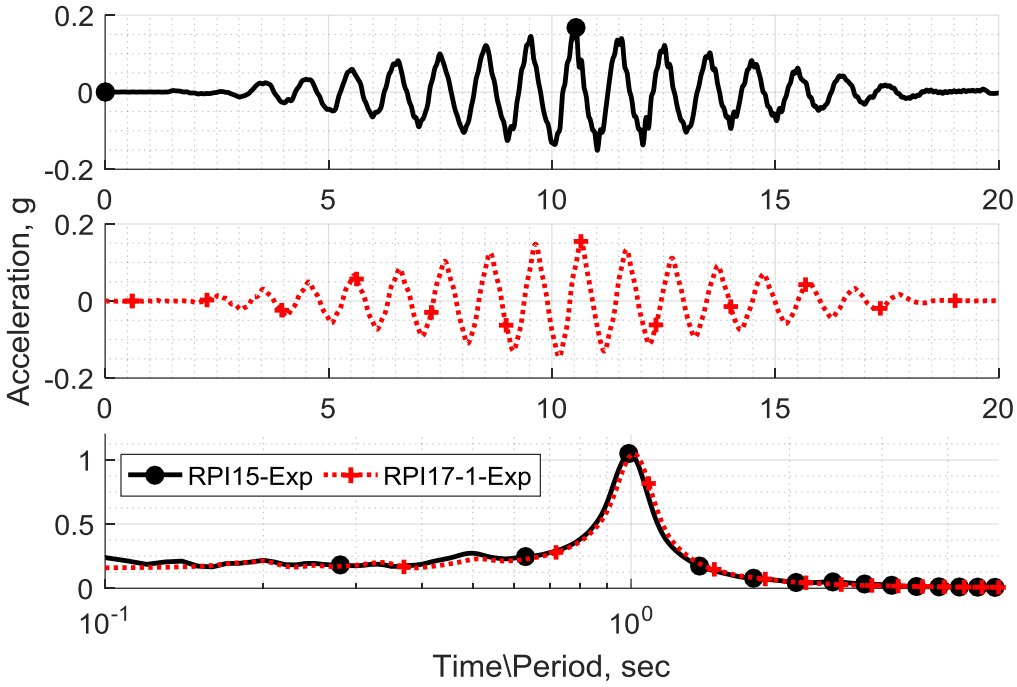

Figure 10: RPI 2015 and 2017 achieved base motions [50,51]

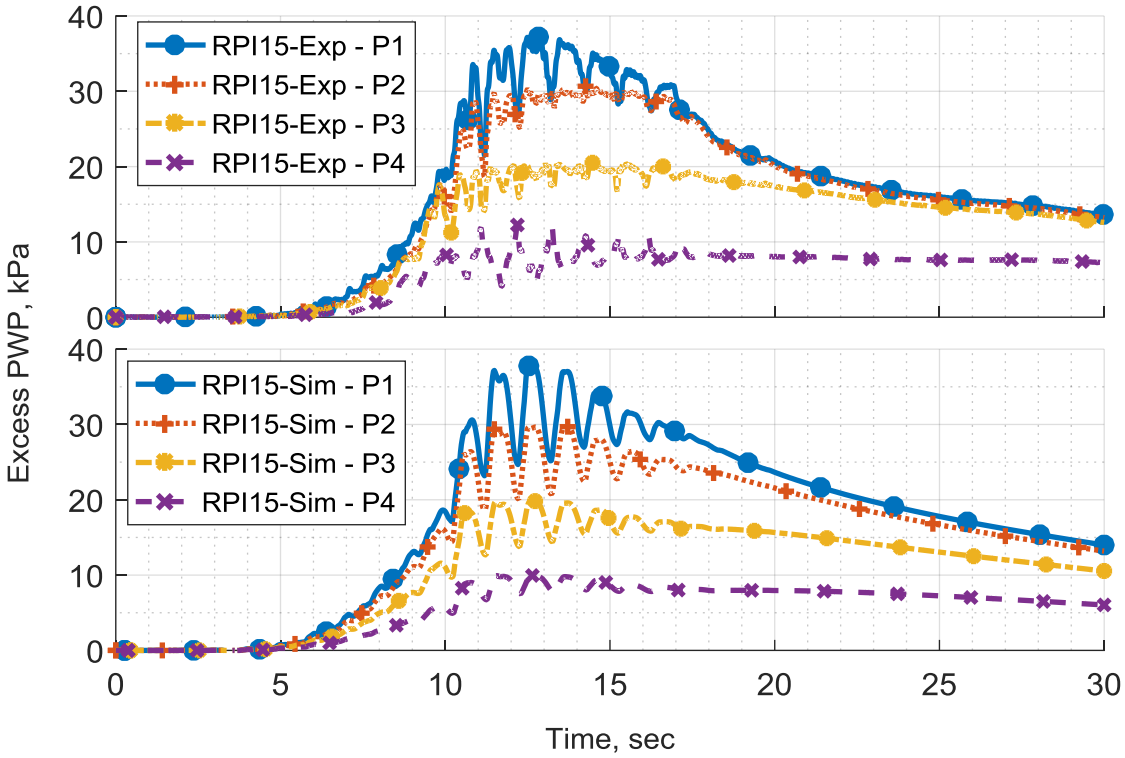

Figure 11: RPI15 excess pore pressure development at the central sensor array

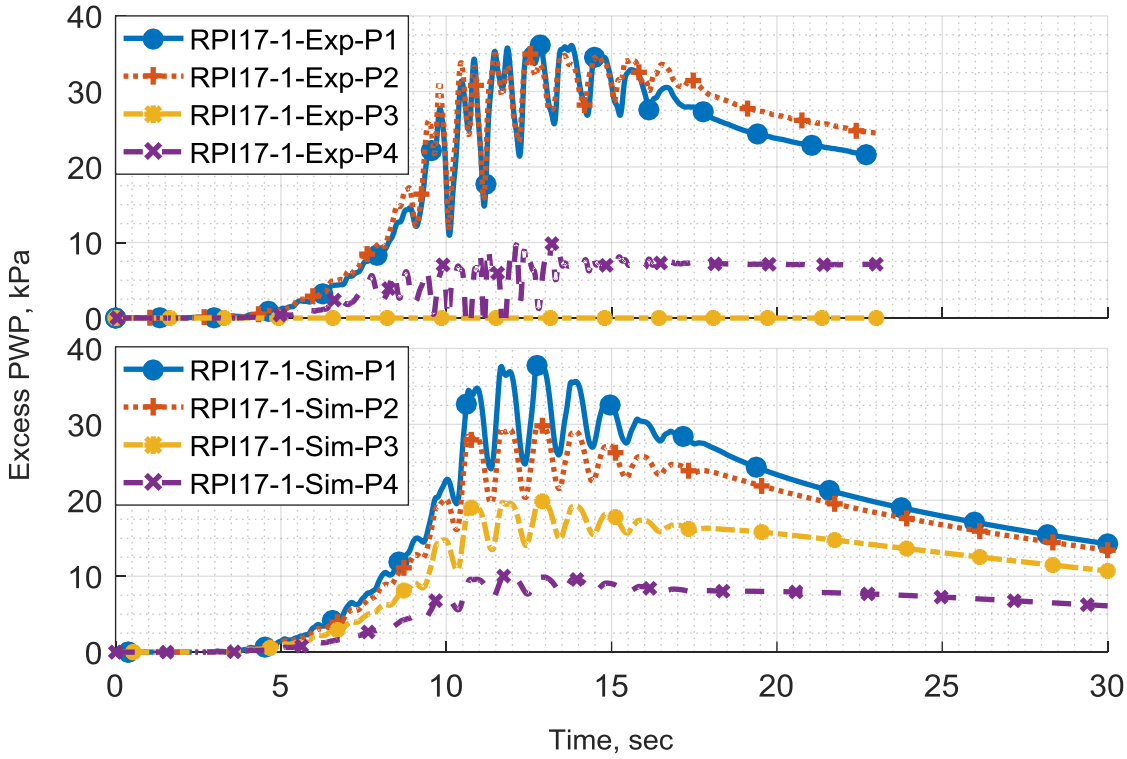

Figure 12: RPI17-1 excess pore pressure development at the central sensor array

The soil lateral displacements are compared in Figures 13 and 14 for the RPI15 and RPI17-1 experiments. Again, the numerical simulations were able to closely capture the final lateral displacement for both experiments. However, the simulations produce much lower dynamic displacements than what were measured for both experiments. While this is an important discrepancy and must be addressed in future developments of the model, the trend and maximum value of lateral spreading were considered as the key parameters of soil response in this study.

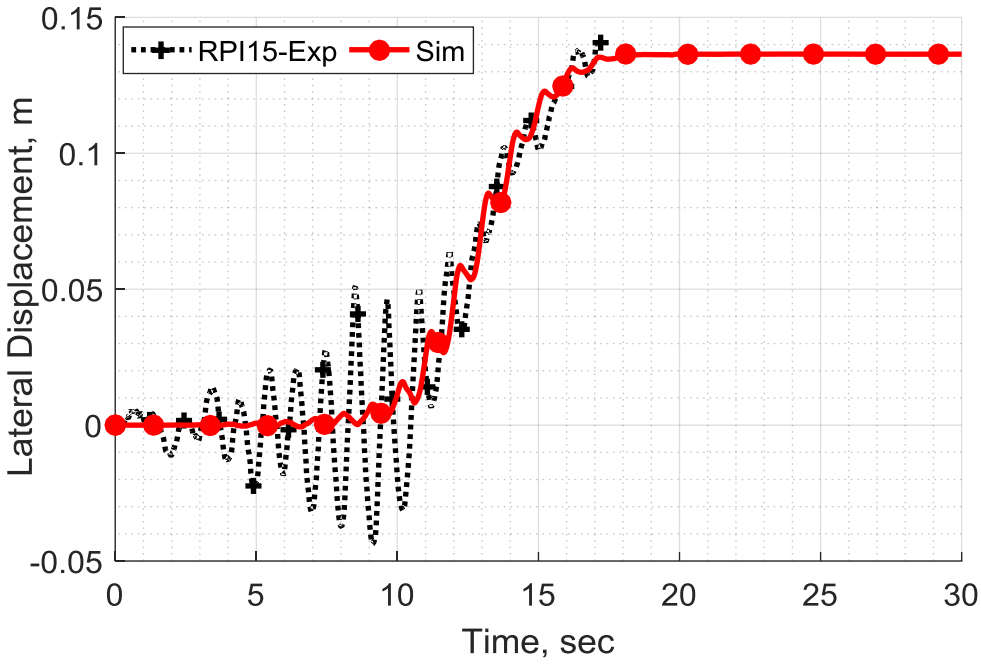

Figure 13: RPI15 Lateral displacement time history at the center of the ground surface

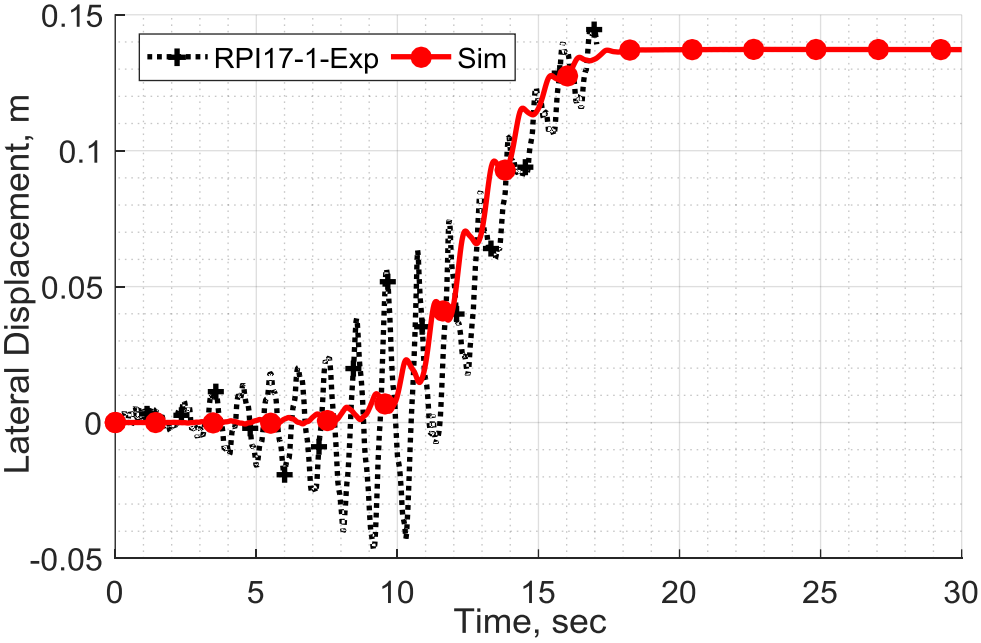

Figure 14: RPI17-1 Lateral displacement time history at the center of the ground surface

Table 6 shows a summary of the lateral displacement at the end of the dynamic motion for all RPI experiments along with the simulation results. The last column of the table shows the percent error between the measured displacement and simulation results. This provides a measure of how well the simulation captured the experiment.

Table 6: RPI Centrifuge Experiments Summary of Displacements

Experiment	Measured Displacement (m)	Simulation Results (m)	% Error
RPI15	0.141	0.136	3.5
RPI17-1	0.145	0.137	5.5

4. Consequences of Spatial Variability of Soil Density

The variability of the soil density in the centrifuge specimen was analyzed before the LEAP-UCD-2017 experiments were conducted. Therefore the assumed statistics in this study are based on the LEAP-GWU-2015. During the LEAP-GWU-2015 the achieved dry densities had a range of variation of 108 kg/m^3 [38]. The target dry density was 1650 kg/m^3 which corresponded to a void ratio of 0.606. Therefore this void ratio was assumed to be the average void ratio and the coefficient of variation was assumed to be 7.8% corresponding to the observed range of variation. These assumptions are also supported by the finding of Lacasse and Nadim [2] in which they reported that the initial void ratio of soils in the field can be represented with a normal distribution with a coefficient of variation ranging from 7 to 30 percent. Later on, the LEAP-UCD-2017 experiments showed that the achieved density corresponded to an average void ratio of 0.603 and a coefficient of variation of 4.63%.

There are several ways to model the observed variability in soil density. The first one considered here assumes that the variability density is an epistemic variability which corresponds to the accuracy of the measurements and the consistency of the specimen preparation. In this case, the assumed statistics of the void ratio pertains to the void ratios reported for a uniform sample with a constant void ratio throughout the soil layer.

The second approach takes into account the spatial variability that may be present within the test specimen. As mentioned in section 1, the spatial variability could be split into a trend component and a random component. The presence or absence of a trend in the achieved soil density depends on the preparation method used to set up the specimen. In the LEAP tests, the specimens were prepared by dry pluviation. If the sand was poured from the same position until the model is setup then it safe to assume that the soil density is higher at the base of the specimen and lower at the top surface. Thus there is a trend present for the soil density and void ratio. On the other hand, if the sand was poured from the same distance to the surface there will be no trend. For the cases where a trend is present the following relationship was assumed to describe the mean value of the void ratio,

$$\mu_e = 0.559 + 0.024z \quad (1)$$

Where z is the depth from the soil surface. Equation -1 assumes a mean void ratio of 0.606 at the center of the soil layer while the slope of the trend corresponds to the assumed range of variation.

To include the random component of the spatial variability, the effect of the spatial correlation needs to be considered. Two cases are considered here. The first case assumes no spatial correlation within the random field. The second one considers the presence of spatial correlation.

A correlated multivariate Gaussian process has a probability density function as shown in Eq.-2.0 [7]:

$$f_{\mathbf{x}}(\mathbf{x}) = \frac{1}{\sqrt{(2\pi)^k |\mathbf{C}|}} \exp\left\{-\frac{1}{2}(\mathbf{x}-\boldsymbol{\mu})^T \mathbf{C}^{-1}(\mathbf{x}-\boldsymbol{\mu})\right\} \tag{2}$$

Where, the random variables vector **x** has a mean of vector **μ** and a covariance matrix **C** that are computed as,

$$\boldsymbol{\mu} = E[\mathbf{X}]; \qquad \mathbf{C} = E\left[(\mathbf{X}-\boldsymbol{\mu})(\mathbf{X}-\boldsymbol{\mu})^T\right] \tag{3}$$

Since a stationary random process is assumed, the covariance matrix is independent of position and can be represented in terms of the correlation coefficient **ρ**,

$$\mathbf{C} = \boldsymbol{\rho}\boldsymbol{\sigma}_{\mathbf{x}}^2 \tag{4}$$

In this work, the correlation coefficient is modeled using an exponential function as shown in Eq. -5.0 [7]:

$$\rho_{ij} = \exp\left(-\frac{1}{2}\left[\frac{|x_i - x_j|}{\theta_x} + \frac{|y_i - y_j|}{\theta_y}\right]\right) \tag{5}$$

Where x and y represent the coordinate position for the i^{th} and j^{th} random variable. θ_x and θ_y are the correlation lengths in the *x* and *y* directions, respectively.

The random field generation relies on the use of the eigenvector and eigenvalues of the covariance matrix. A correlated random field can be modified to a series of uncorrelated random variables,

$$\mathbf{Q}\mathbf{C}\mathbf{Q}^T = \boldsymbol{\psi} \tag{6}$$

Where **Q** is the eigenvector for the covariance matrix **C** and **ψ** is a diagonal matrix of the variances of the uncorrelated random vector **Z**=**QX**. Using this principle a generated series of uncorrelated random field $\mathbf{Z} \sim N(\mathbf{0}, \mathbf{I})$ can be transformed into a correlated random filed **X**=**QZ**+**μ**

~ N (**μ**, **C**). The formulation for the correlated random field generation has been implemented in Matlab by Constantine and Wang [52].

Table 7 shows the different cases that were analyzed. The first case is called epistemic variability. This case represents the study of the uncertainty pertaining to the errors in measurements. In the LEAP-2015 centrifuge tests, the specimens were prepared by dry pluviation. The difficulty in preparing a sloped soil profile, the inaccuracy in the measurement of the final geometry of the specimen, and the ability of the experimenter to keep the height of fall constant during the pluviation process usually leads to variability in the reported achieved dry density. Hence, the first set of stochastic simulations investigates the effects of the epistemic variability in the soil dry density (or void ratio). In this case, the initial void ratio is considered as a random variable that is uniformly assigned to the elements within the finite element model.

The remaining four cases in Table 7 consider the effect of spatial variability in the centrifuge specimen. Although centrifuge specimens are prepared in a closed and controlled environment, preparing a specimen with a void ratio that is constant with the depth is rather difficult. For the second stochastic analysis, Spatial–1 case, the initial void ratio is considered to be a Gaussian random field. The mean value of the initial void ratio is assumed to be dependent on depth with a higher void ratio closer to the surface representing looser soil conditions and a lower void ratio at the base representing a denser soil. A constant coefficient of variation is considered (the same value as the one used in the first stochastic analysis). The random field is considered to be spatially uncorrelated. Figure 15, shows the contour plot for the distribution of the initial void ratio for a single realization of Spatial–1 case. The empirical cumulative probability distributions of the initial void ratio for all the realizations in this case are presented in Figure 16.

Table 7: Spatial Variability Stochastic Analysis Cases

Analysis	Mu	C.O.V	θ_x	θ_y
Epistemic	0.606	7.78%	Uniform	
Spatial–1	0.5588+0.0244y	7.78%	0	0
Spatial–2	0.5588+0.0244y	7.78%	5.0	0.5
Spatial–3	0.606	7.78%	5.0	0.5
Spatial–4 $0.601<\mu_g<0.611$	0.606	7.78%	5.0	0.5

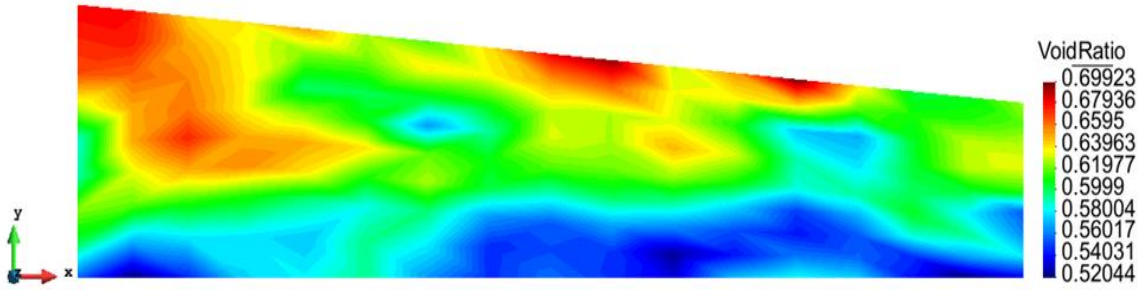

Figure 15: Distribution of Initial Void Ratio of a Single Realization of the Spatial- Analysis

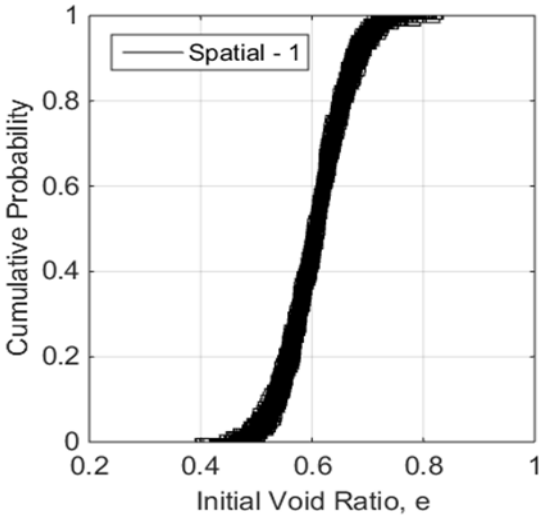

Figure 16: Cumulative Distribution of Initial Void Ratios for Spatial-1 Analysis

For Spatial–1 case, the random field is taken to be spatially uncorrelated. Although this assumption is unrealistic for soil properties, it is a reasonable starting point when no additional information is available on the spatial correlation of the random field. The spatial correlation of the initial void ratio is influenced by many factors. In the field, the initial void ratio is influenced by the weathering, sedimentation, and transportation as well as the stress history of the soil deposit among other factors. While in a centrifuge experiment, the initial void ratio is influenced by the sample preparation technique, saturation, and consolidation processes as well as proximity to the soil box boundaries. Since each of these factors affect the spatial correlation, estimating the spatial correlation of void ratio is rather difficult and any estimation requires experimental data for it to be validated.

While it remains difficult to model the exact degree of spatial correlation in the initial void ratio, in this study the effects of the presence of spatial correlation is investigated. In case 3, Spatial – 2, the initial void ratio is assumed as a stationary Gaussian random field with the same mean and coefficient of variation as Spatial–1 case. However, in this case, spatial correlation is considered. For Spatial–2 case, Figure 17 shows the contour plot of the initial void ratio for a single realization. Figure 18 shows the empirical cumulative probability distribution for all the realizations in this case.

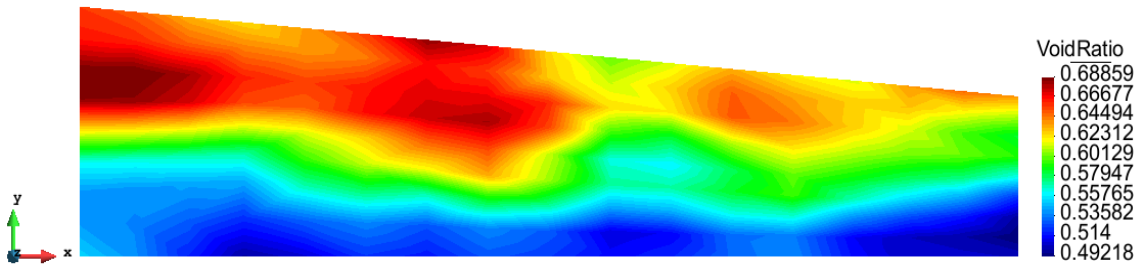

Figure 17: Distribution of Initial Void Ratio of a Single Realization of the Spatial-2 Analysis

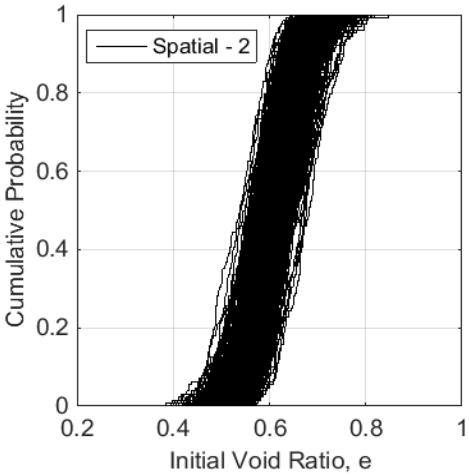

Figure 18: Cumulative Distribution of Initial Void Ratios for Spatial-2 Analysis

In the spatial–3 case, the random field is assumed to have a constant mean. This case resembles the situation in which a constant drop height dry pluviation is used for sample preparation. The same method of random field generation is used as in spatial–2 case. While a constant mean of 0.606 is assumed, the same spatial correlation lengths of 5.0 and 0.5 were assumed in the x and y directions respectively. Figure 19 shows the contour plot of the initial void ratio for a single realization. Figure 20 shows the empirical cumulative probability distribution for all the realizations in this case.

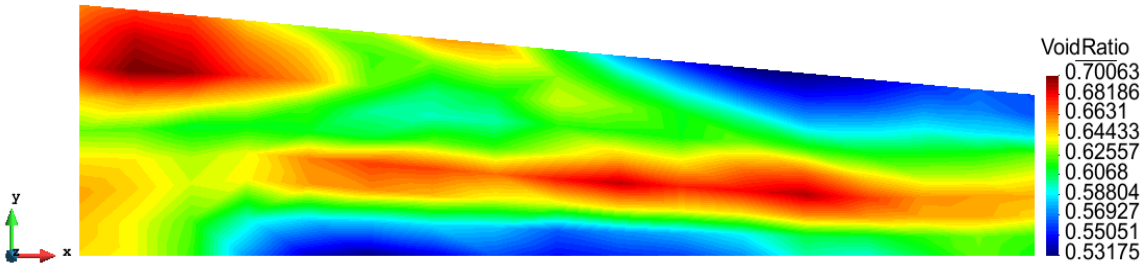

Figure 19: Distribution of Initial Void Ratio of a Single Realization of the Spatial -3 Analysis

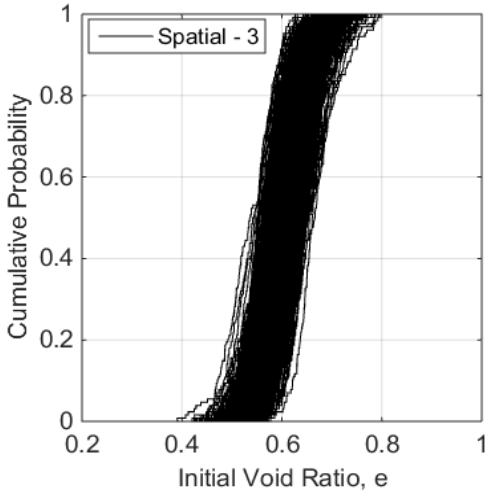

Figure 20: Cumulative Distribution of Initial Void Ratios for Spatial-3 Analysis

The mean and coefficient of variability in Table 7 pertain to the random variables within the Gaussian random field. While these parameters apply to each random variable separately during the random field generation, it is not guaranteed that the global mean and coefficient of variation for each realization to be the same. This can be observed in Figures 16, 18 and 20 where the cumulative distributions have different bandwidths reflecting variability in the mean and coefficient of variation of the centrifuge model specimen due to the spatial correlation. However, in a laboratory condition, the global mean and standard deviation are more controlled. In the last case, spatial–4, the global mean of the initial void ratio of the model, μ_g is controlled by limiting it to the range of $0.601<\mu g<0.611$. With this limitation, the rest of the parameters were set to be equal to those used in spatial – 3 case. Figure 21 shows the contour plot initial void ratio for a single realization. Figure 22, shows the empirical cumulative probability distribution for all the realizations in this case. It can be seen from Figure 22 that by setting a limit on the global mean, the bandwidth of the cumulative distribution became narrower.

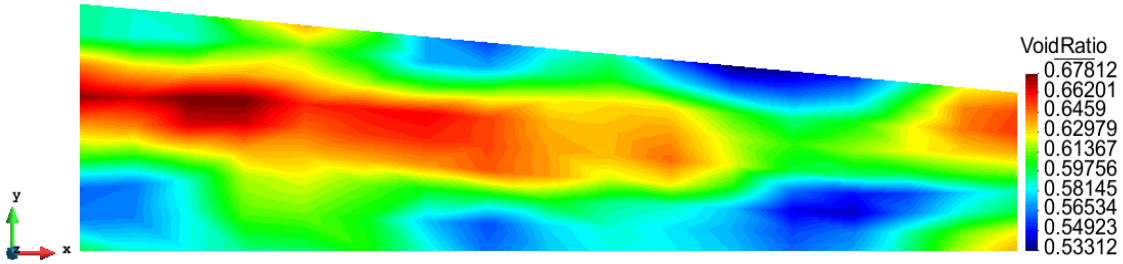

Figure 21: Distribution of Initial Void Ratio of a Single Realization of the Spatial-4 Analysis

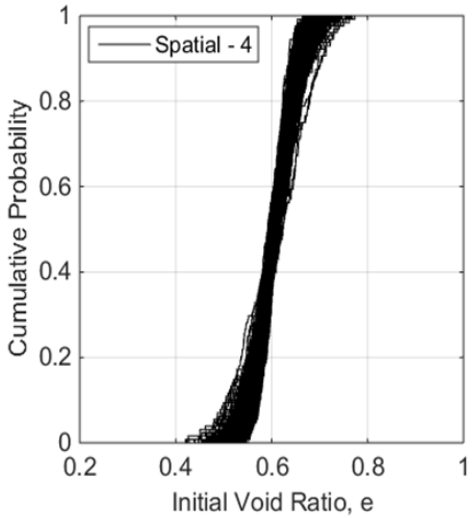

Figure 22: Cumulative Distribution of Initial Void Ratios for Spatial-4 Analysis

The above five cases of stochastic analyses were performed using the same finite element setup used in the deterministic analysis. The variability is introduced in each simulation through initial void ratio, soil density, and permeability of each element. The permeability was obtained using the relationship between the void ratio and permeability, Eq. 7, obtained from the hydraulic

conductivity tests performed on Ottawa F65 sand [46,47]. Each analysis consisted of 500 simulations.

$$k(cm/s) = 0.0207\, e_o - 0.0009 \tag{7}$$

The results of the above mentioned analyses are presented in the following sections.

4.1.1. Excess Pore Pressure Development

Figures 23 to 27 show the excess pore water pressure time histories computed at a point near the bottom and at the center of the soil specimen where the pore pressure sensors P1 and P3 are placed. The results are illustrated in terms of the mean, the mean plus (or minus) one standard deviation, and the range of the simulations results for the Epistemic case. The dashed horizontal line on each plot indicates the initial vertical effective stress at the locations of P1 and P3. The initial vertical effective stresses were computed based on the reported average density of Ottawa sand, i.e. 1650 kg/m3. Since the initial void ratio is variable within the soil specimen, the corresponding density is variable and the actual initial vertical stress will vary accordingly.

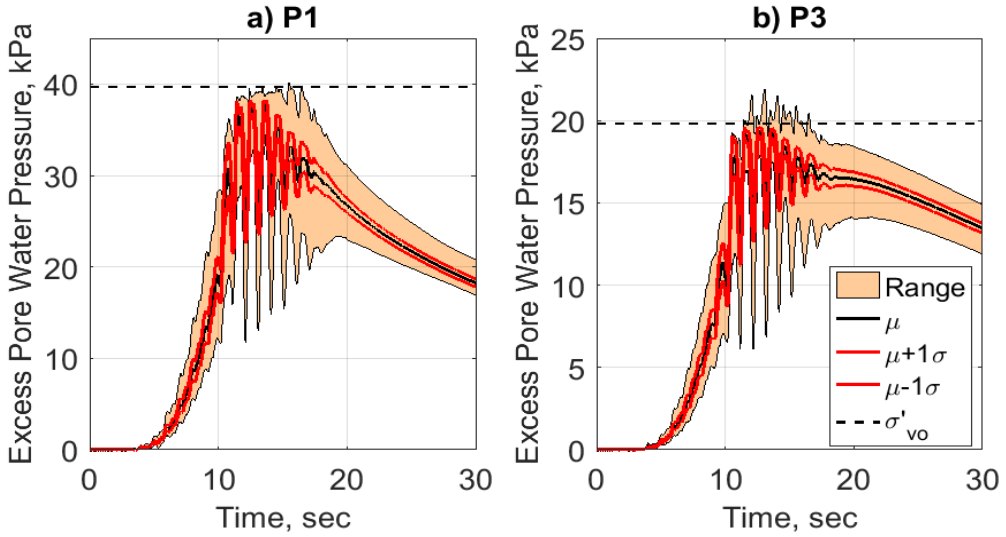

Figure 23: Excess Pore Pressure computed at the Location of P1 and P3 for Epistemic Analysis

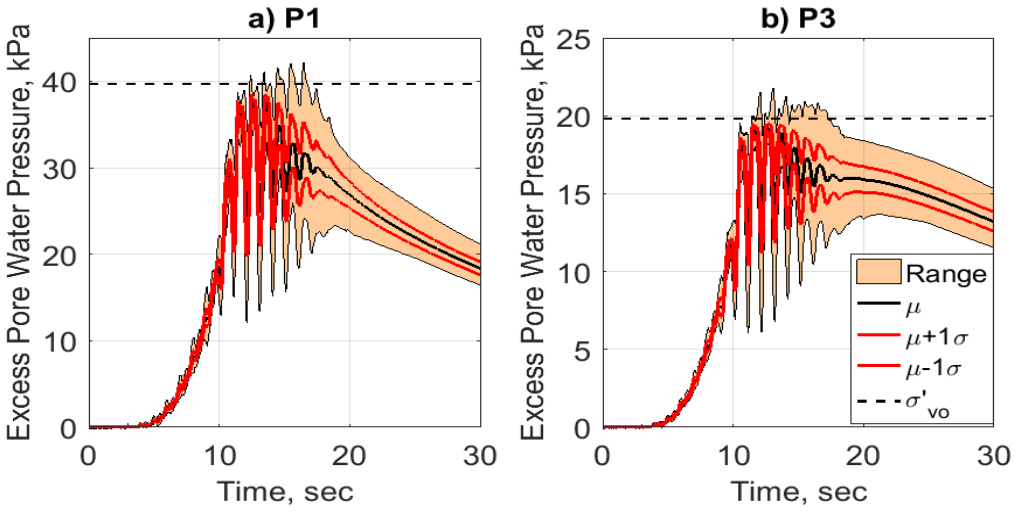

Figure 24: Excess pore pressure computed at the location of P1 and P3 for Spatial–1 Analysis

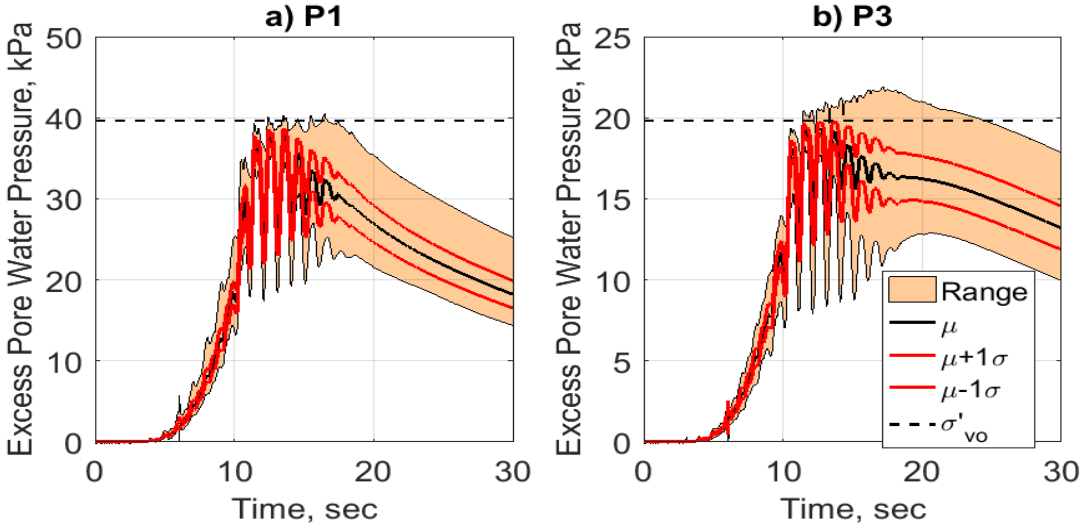

Figure 25: Excess Pore Pressure computed at the Location of P1 and P3 for Spatial–2 Analysis

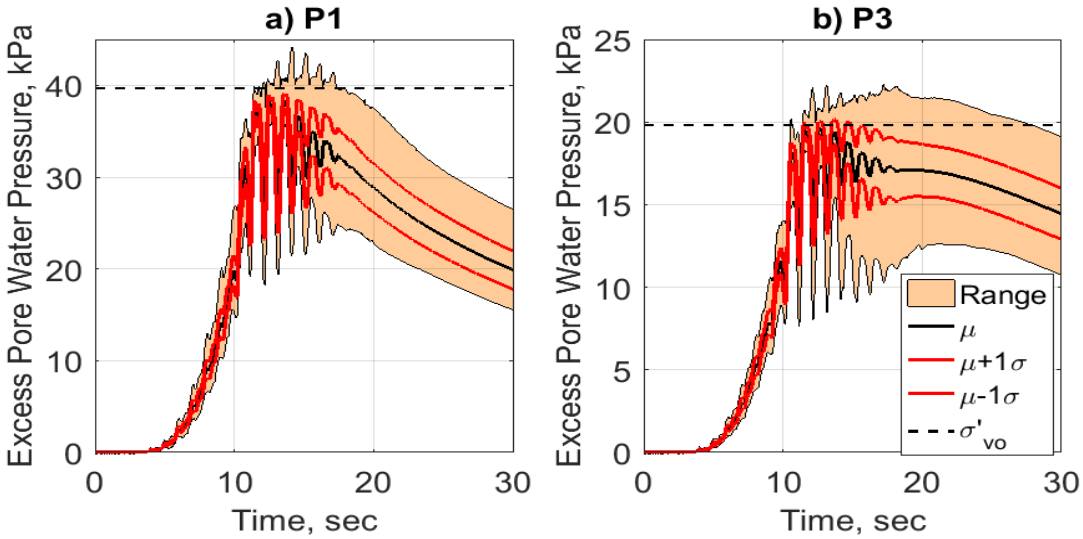

Figure 26: Excess Pore Pressure computed at the Location of P1 and P3 for Spatial–3 Analysis

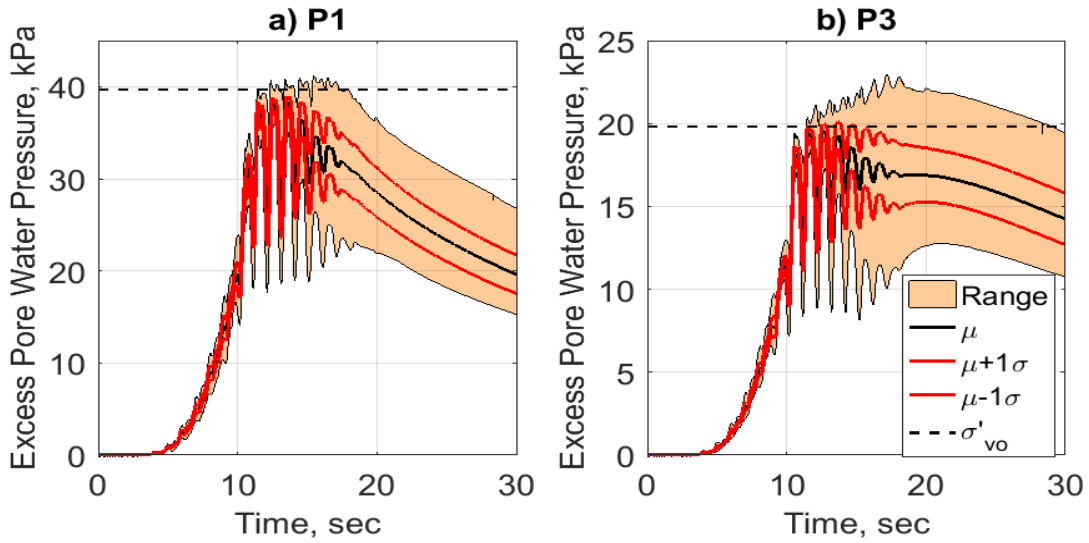

Figure 27: Excess Pore Pressure computed at the Location of P1 and P3 for Spatial–4 Analysis

4.1.2. Surface Displacement

Figures 28 to 32 show the surface settlement and lateral displacement time histories at the top of slop (3.5 meters away from the walls of the soil box) and at the center of slope, respectively. Table 8 shows a summary of the statistics of the final displacements for these time histories.

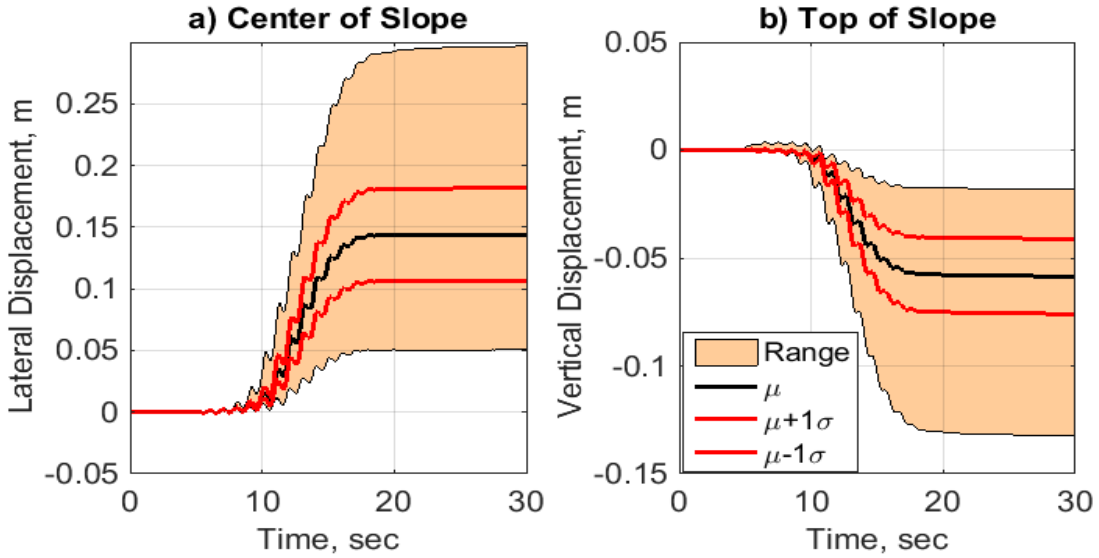

Figure 28: a) Surface Lateral Displacement at the Center of Slope b) Surface Settlement at the Top of Slope for the Epistemic Analysis

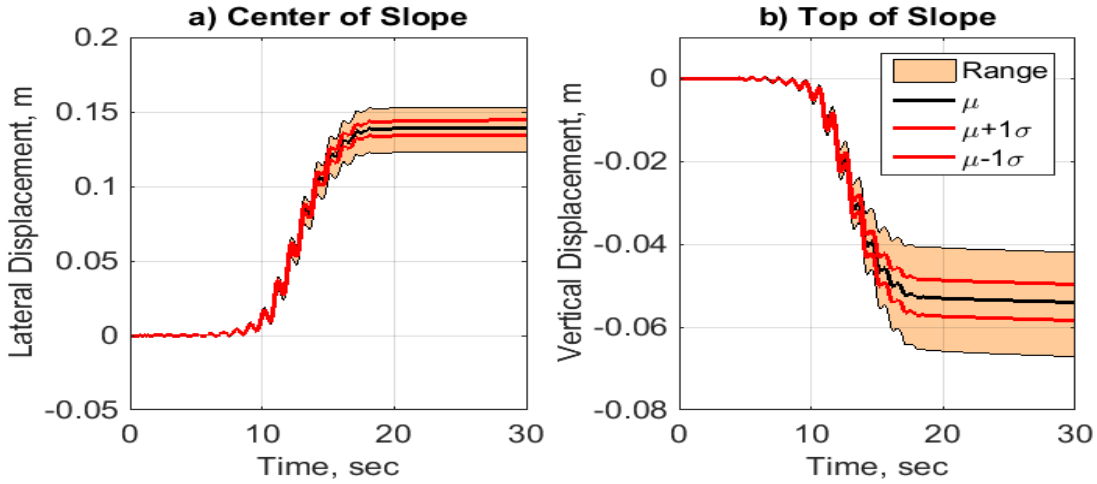

Figure 29: a) Surface Lateral Displacement at the Center of Slope b) Surface Settlement at the Top of Slope for the Spatial–1 Analysis

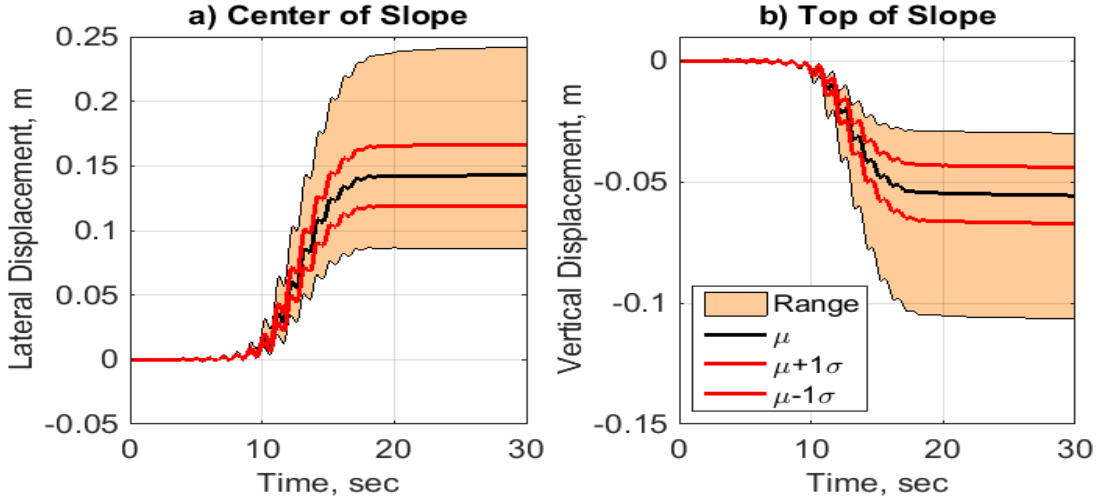

Figure 30: a) Surface Lateral Displacement at the Center of Slope b) Surface Settlement at the Top of Slope for the Spatial–2 Analysis

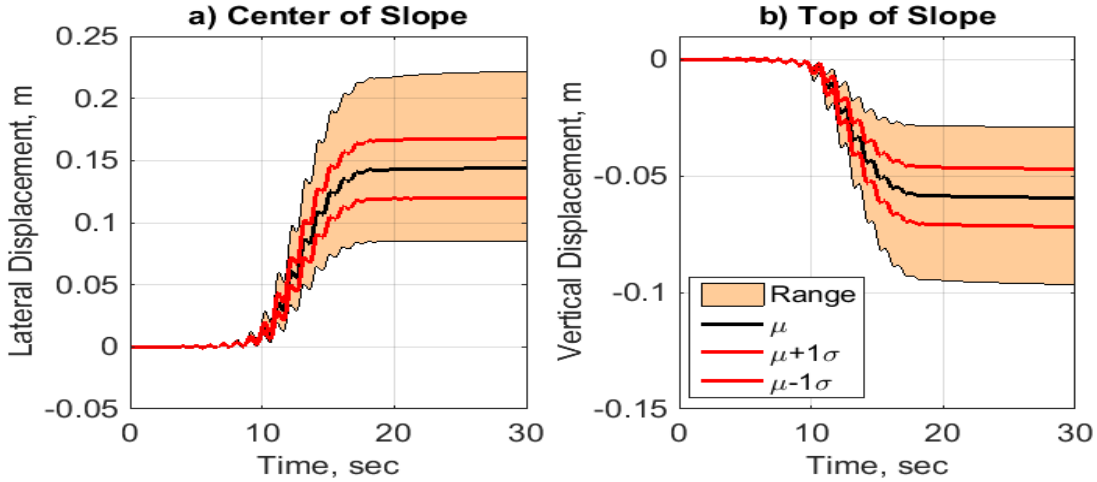

Figure 31: a) Surface Lateral Displacement at the Center of Slope b) Surface Settlement at the Top of Slope for the Spatial–3 Analysis

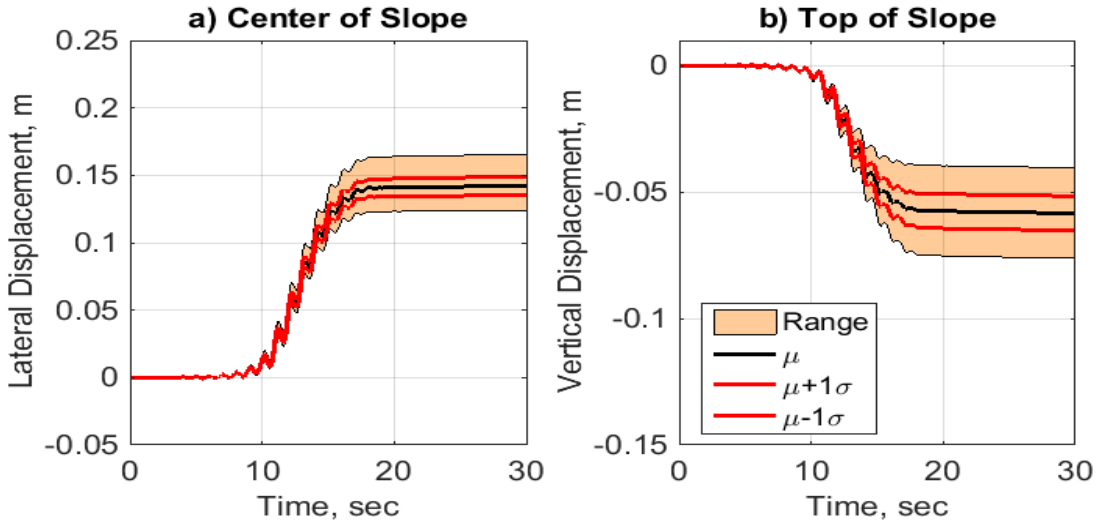

Figure 32: a) Surface Lateral Displacement at the Center of Slope b) Surface Settlement at the Top of Slope for the Spatial–4 Analysis

Table 8: Statistics of the Final Displacements

	Lateral Displacement		Settlement	
Analysis	μ (m)	COV (%)	μ (m)	COV (%)
Epistemic	0.1440	26.18	0.05860	29.59
Spatial – 1	0.1395	3.50	0.05398	8.06
Spatial – 2	0.1427	16.75	0.05554	20.90
Spatial – 3	0.1438	16.69	0.05941	20.82
Spatial - 4	0.1418	4.80	0.05830	11.66

4.1.3. Lateral Spreading Soil Profile

Figures 33 to 37 show the lateral displacements of the points located on the central line of the soil specimen. The results of the finite element analyses for soil specimens with uniform initial void ratios corresponding to various percentiles of the target distribution are also shown in these plots.

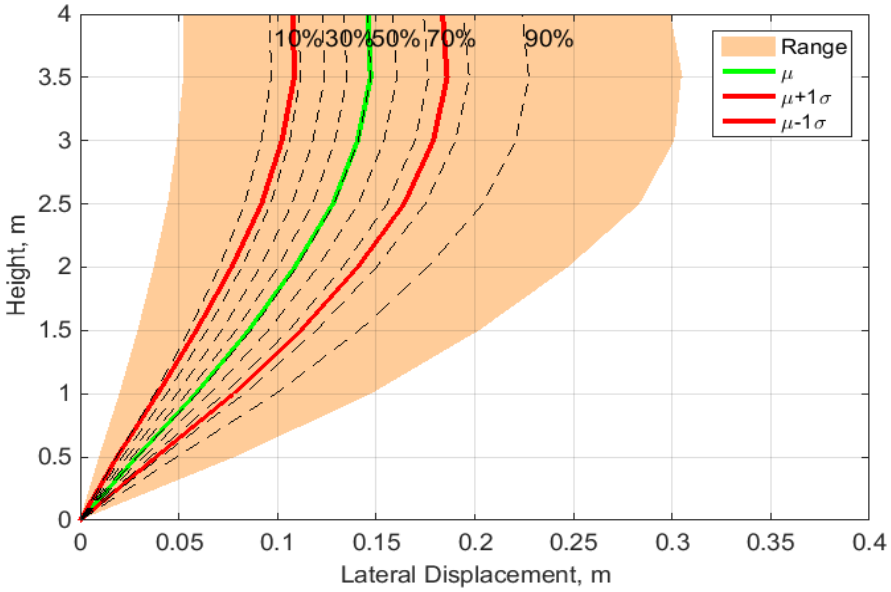

Figure 33: Comparison of Soil Lateral Displacements at the Center of the Model computed for the Epistemic Analysis and the Uniform Models corresponding to different percentiles of the initial void ratio for the target distribution

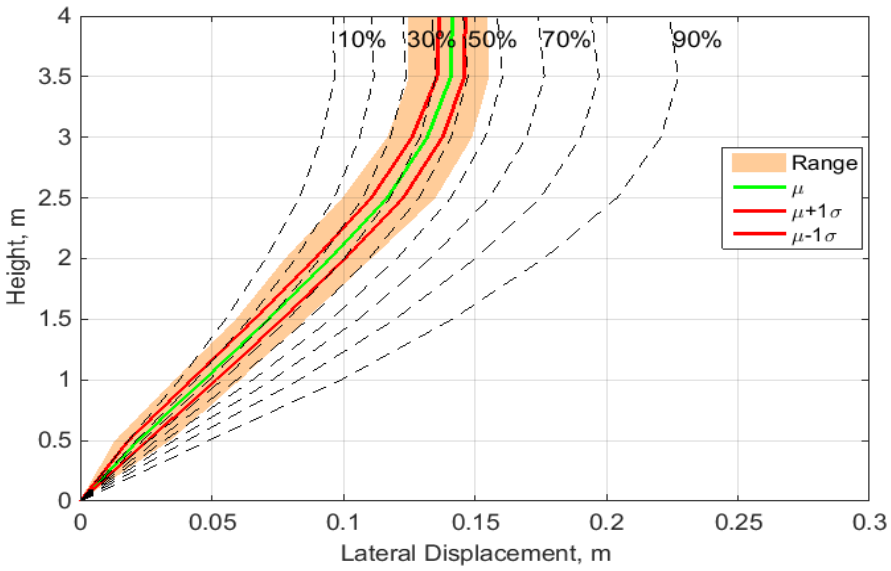

Figure 34: Comparison of Soil Lateral Displacements at the Center of the Model computed for the case with Spatial – 1 Analysis and the Uniform Models corresponding to different percentiles of the initial void ratio for the target distribution

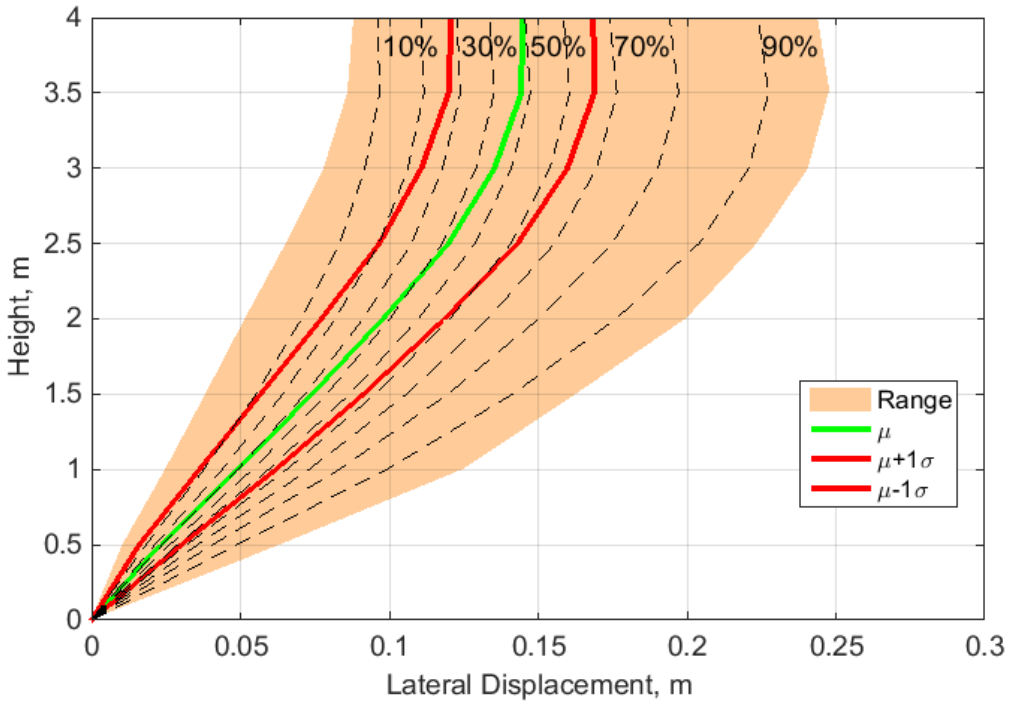

Figure 35: Comparison of Soil Lateral Displacements at the Center of the Model computed for the case with Spatial – 2 Analysis and the Uniform Models corresponding to different percentiles of the initial void ratio for the target distribution

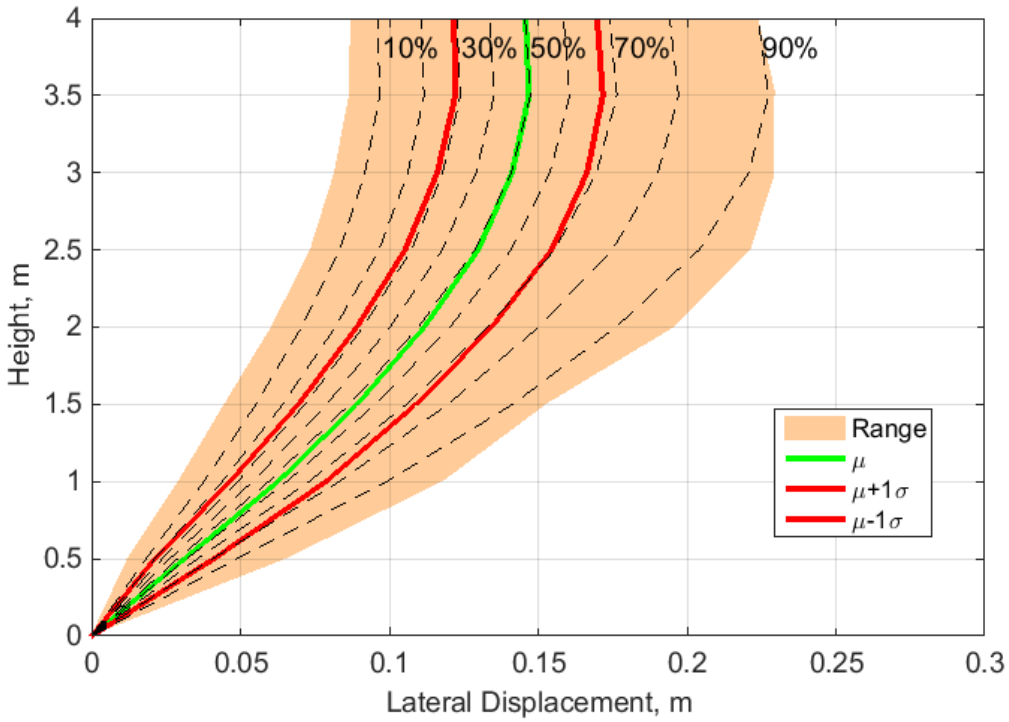

Figure 36: Comparison of Soil Lateral Displacements at the Center of the Model computed for the case with Spatial – 3 Analysis and the Uniform Models corresponding to different percentiles of the initial void ratio for the target distribution

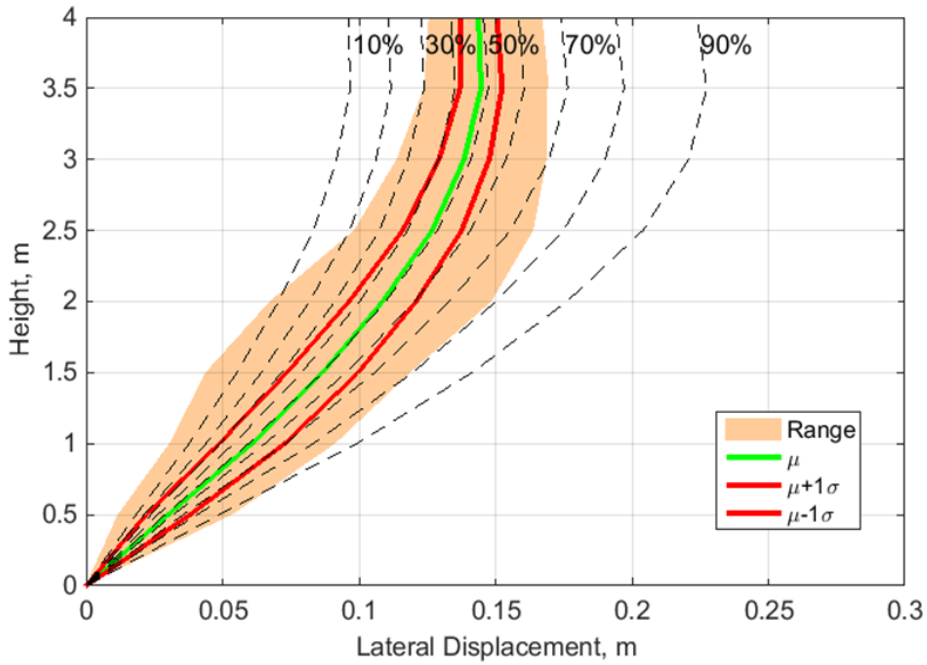

Figure 37: Comparison of Soil Lateral Displacements at the Center of the Model computed for the case with Spatial – 4 Analysis and the Uniform Models corresponding to different percentiles of the initial void ratio for the target distribution

4.1.4. Discussion

The results shown in Figures 23 to 27 indicate that the mean excess pore water pressure obtained for the epistemic and spatial variability analyses are similar in terms of the maximum excess pore pressure generated, and the rates of generation and dissipation. However, the range of variability in these cases is different especially during the dissipation phase. A clear comparison can be seen in Figures 38 and **Error! Reference source not found.**39 in which the mean and standard deviation of excess pore pressure time histories for each of the analysis cases are plotted. These plots confirm the observed trend of the mean excess pore pressure time history shown in Figures 23 to 27. The standard deviation plots show that the epistemic analysis exhibits larger variability during the pore pressure generation phase. However, the epistemic analysis showed the smallest variability during the dilative and dissipation phases. For the spatial variability analyses, higher variability was observed in the dilative phase. During the generation phase, the average void ratio of the centrifuge specimen has an effect on the degree of variability. The cases of Spatial – 1 and Spatial–4 have a smaller variability in the mean void ratio which is reflected in the narrower bandwidth of the CDF plots shown in Figures 16 and 22. These cases have smaller variability during the generation phase as can be seen in Figures 38 and 39. For the dissipation phase, the Figures show that the presence of a trend in the definition of the random field results in lower variability, while the presence of spatial correlation results in more variability in the excess pore pressure. It can also be seen that the average void ratio of the centrifuge specimen does not affect

the rate of dissipation since both the Spatial–3 and Spatial–4 cases have the same standard deviation during this phase.

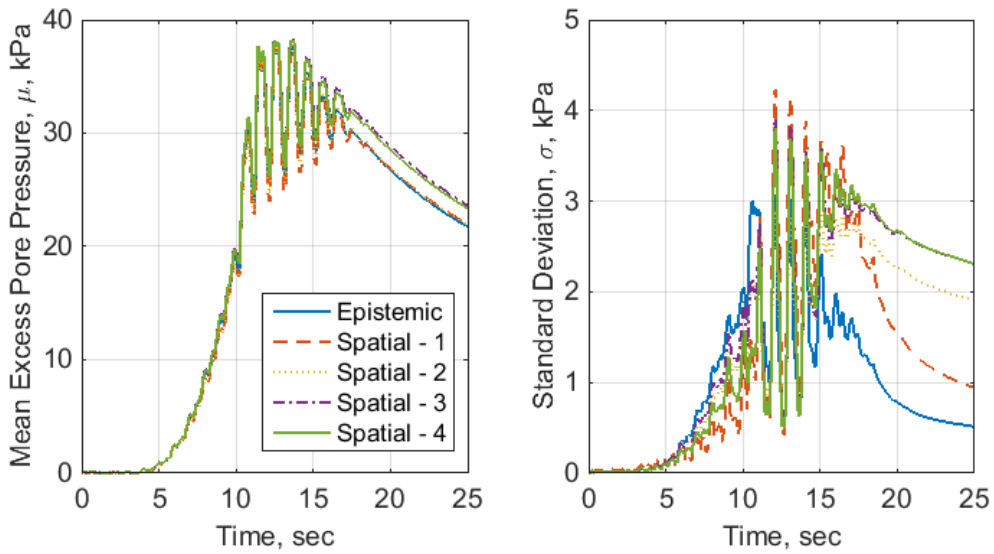

Figure 38: Mean and Standard Deviation of Excess Pore Pressure Time History at P1

Figures 28 to 32 show smaller variability for the lateral displacement and settlement in the Spatial – 1 and Spatial – 4 cases. The largest variability is seen in the epistemic analysis. Table 8 shows a summary of the statistics of the final lateral displacement and settlement for each case. The results summarized in this Table confirm that the mean responses are similar to those observed in Figures 28 to 32. The coefficient of variation shown in Table 8 confirms the observation of the variability of responses in each case. From these results, it can be seen that the variability in the average void ratio of the centrifuge specimen has the most significant effect on the final lateral displacements of the soil. Spatial–1 and Spatial–4 cases showed smaller coefficient of variation as they had the smallest variation in the initial void ratio. The results of Spatial –2 and Spatial–3 cases show that the dependency of the mean void ratio on depth does not affect the final lateral displacement.

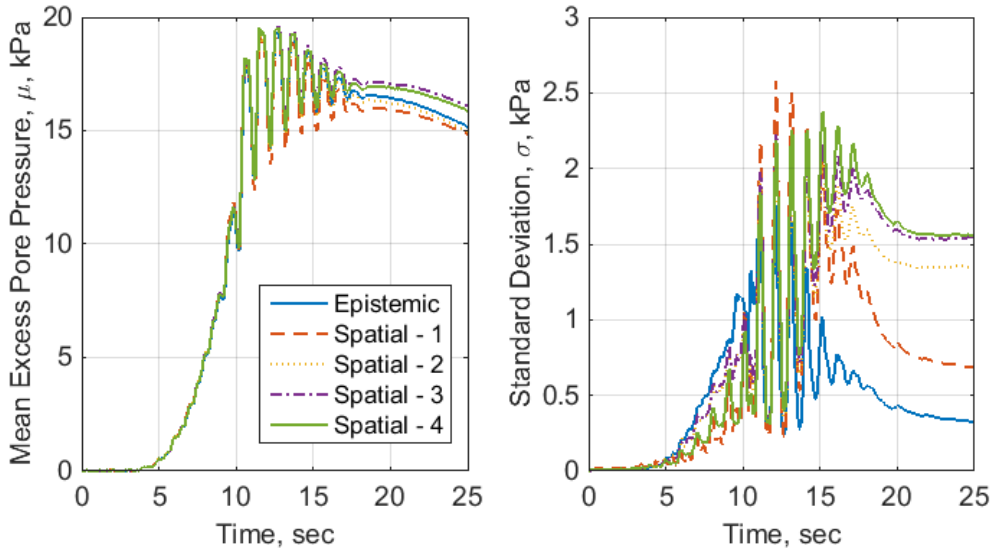

Figure 39: Mean and Standard Deviation of Excess Pore Pressure Time History at P3

Figures 33 to 37 show the average response of the soil profile for the different cases analyzed in this work. Figure 34 shows that the average response of the soil profile in the spatial–1 analysis corresponds to the response of a soil specimen with a uniform initial void ratio that falls between the 20th and 30th percentile of the target distribution for the locations deeper than 2.5 m. For depths of 1.3m to 2.5m the soil response corresponds to response of a soil with a uniform initial void between the 30th and 40th percentile of the target distribution. Similarly for the soil with depth less than 1.3m the soil response corresponds to that with a uniform initial void ratio between the 40th and 50th percentile of the target distribution. Figure 35 shows that the average response of the soil profile in the spatial – 2 analyses corresponds to the response of a soil specimen with a uniform initial void ratio of 30th percentile of the target distribution for the locations deeper than 3.0 m. For depths of 1.75m to 3.0m the soil response corresponds to the response of a soil with a uniform initial void between the 30th and 40th percentile of the target distribution. Similarly for the depths less than 1.75m the soil response corresponds to that with a uniform initial void ratio between the 40th and 50th percentile of the target distribution. Figures 33, 36 and 37 show that the average responses of the soil profile for the epistemic, spatial–3 and spatial–4 cases are similar to that of a soil specimen with a uniform initial void ratio corresponding to the 50th percentile of the target distribution. Although the mean response is the same for these analyses the standard deviation showed significant variations.

The presented results show that a relatively small variation in the soil density can have significant effects on the response of liquefiable ground. High variability in the lateral displacement and settlement of the soil can be observed depending on how the variation of density is modeled. Hence a more detailed knowledge of density variation is necessary if a more accurate prediction of the soil response is desired.

5. Consequences of Variability in Base Excitation

During the LEAP-GWU-2015 and LEAP-UCD-2017, a total of 27 centrifuge experiments were conducted. The target base motion consisted of a ramped sinusoidal motion with a frequency of 1Hz. For the majority of the experiments, the target PGA of the input motion was 0.15g. However, the achieved base motion showed variability in the magnitude and frequency content. Figure 40 shows the variations observed in the base motions achieved for 15 of the LEAP centrifuge experiments with a target PGA of 0.15g. Here the base motion was treated as a random process defined by the mean response spectrum (shown in red) and the covariance matrix of the spectral acceleration of the achieved base motions. The achieved PGA for these experiments had a mean value of 0.176 g and a coefficient of variation of 14.4 %.

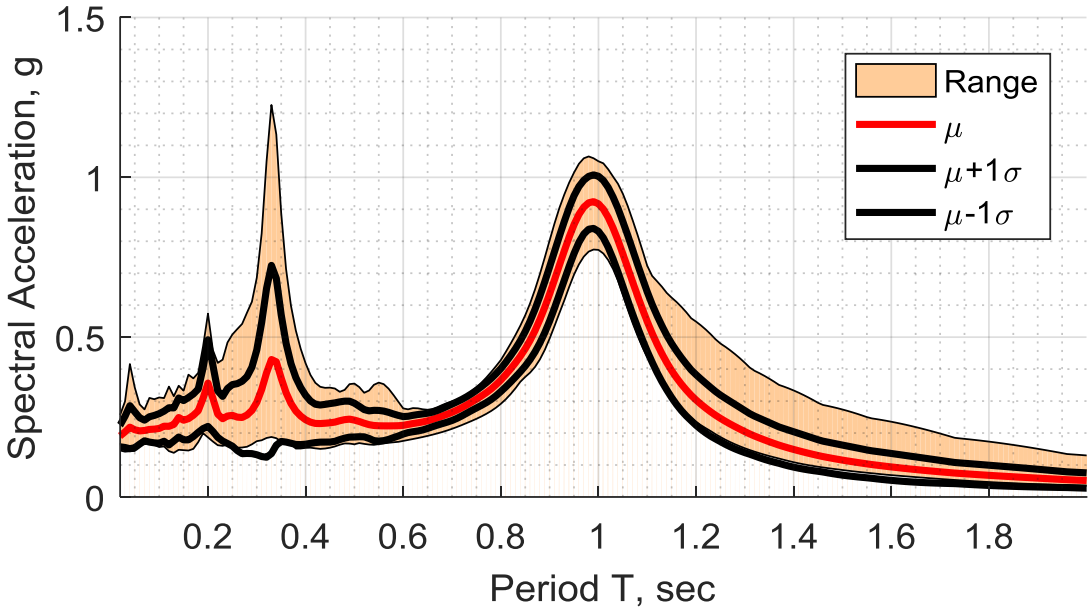

Figure 40: Spectral acceleration of the achieved base motions in LEAP-2015 and 2017 tests (Damping ratio = 5%)

For Monte Carlo simulations, random response spectra were generated using the obtained mean and covariance. Once a random response spectrum was obtained, a corresponding time history base motion was generated iteratively. The generated time history consisted of a set of ramped sinusoidal waves with a frequency in the range of 0.01 to 50 HZ covering the frequencies in the response spectra. The peak amplitude of each wave was obtained iteratively to match the generated response spectrum. The phase angle for each sinusoidal wave was treated as a normally distributed random variable with a zero mean and a standard deviation of $\pi/3$. A sample of 500 base motions was generated. Figure 41 shows two realizations of the generated synthetic base motions. The left figure shows the generated time history, while the right figure shows how the response spectrum of the generated motion compares to the target realization. Figure 42 shows that the response spectra of the generated time histories (Synt.) closely match the response spectra of the base motions achieved in LEAP-2015 and 2017 (exp.).

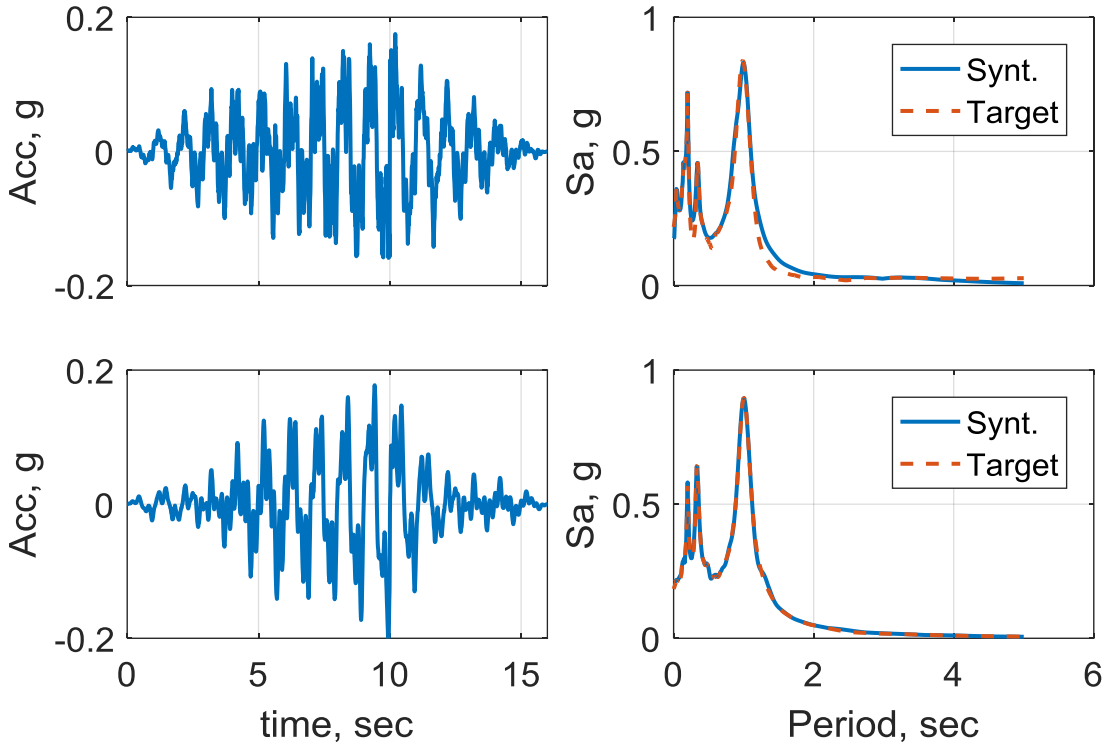

Figure 41: Two realizations of the synthetic input motions generated and their comparison with the target response spectrum

Three cases of the stochastic analysis were conducted depending on how the soil is modeled. The first case studies the effect of the base motion variability solely, therefore the soil was treated as a homogenous layer with a void ratio of 0.606 corresponding to a dry density of 1650 kg/m^3. The second case considers the spatial variability of the soil. In this case, the soil is modeled in the same way as case Spatial-4, Table 7. This case assumes that the average void ratio remains within 1 percent of 0.606. This allows for isolating the effect of the spatial variability from the effect of the variation in the soil density. Finally, the third case considers the combined effect of the soil spatial variability and the mean void ratio variability along with the base motion variability. This case is simulated using the Spatial-3 assumptions in generation of the soil random fields.

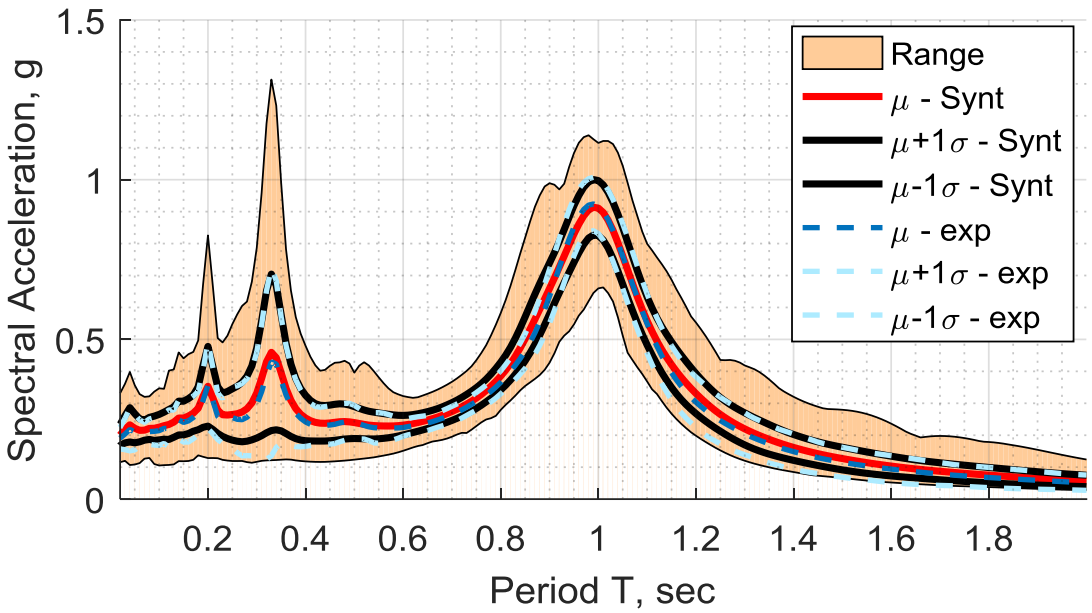

Figure 42: Spectral acceleration of the generated random base motions

5.1.1. Excess Pore Pressure

Figure 43 shows the excess pore pressure at the locations of the pore pressure transducers P1 and P4 (Figure 1) for the homogeneous soil case. The results are presented in terms of the mean, the mean +/- one standard deviation of the results, and the range. The initial vertical effective stress is shown by a dashed line in the figure. Figure 44 shows the development of excess pore pressures for the spatial variability case at the same locations as those shown in Figure 43. Figure 45, shows the excess pore water pressure development for the spatial and mean void ratio variability case.

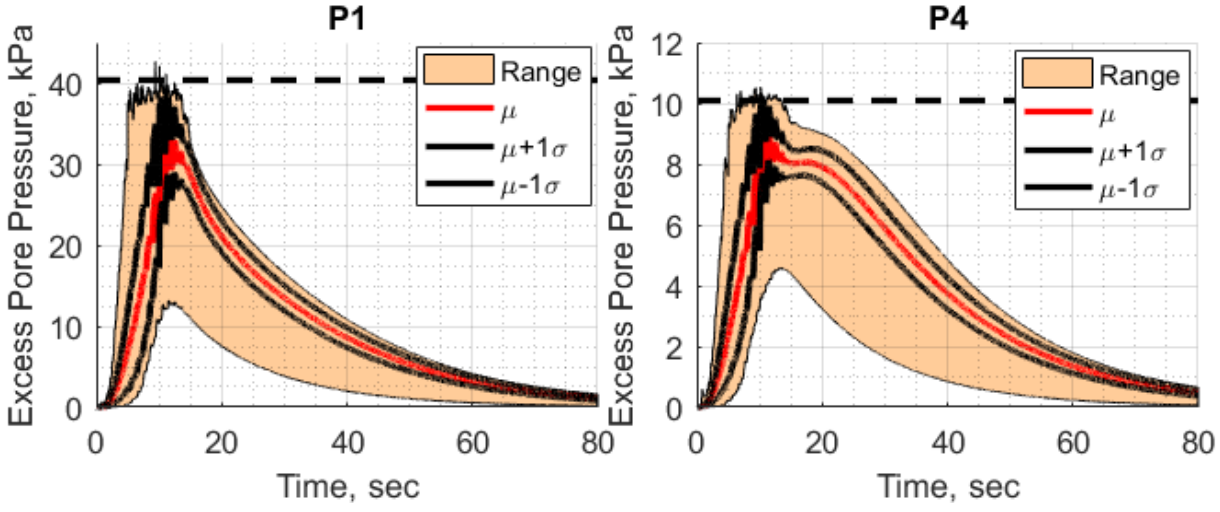

Figure 43: Excess pore pressure ratio for homogeneous case

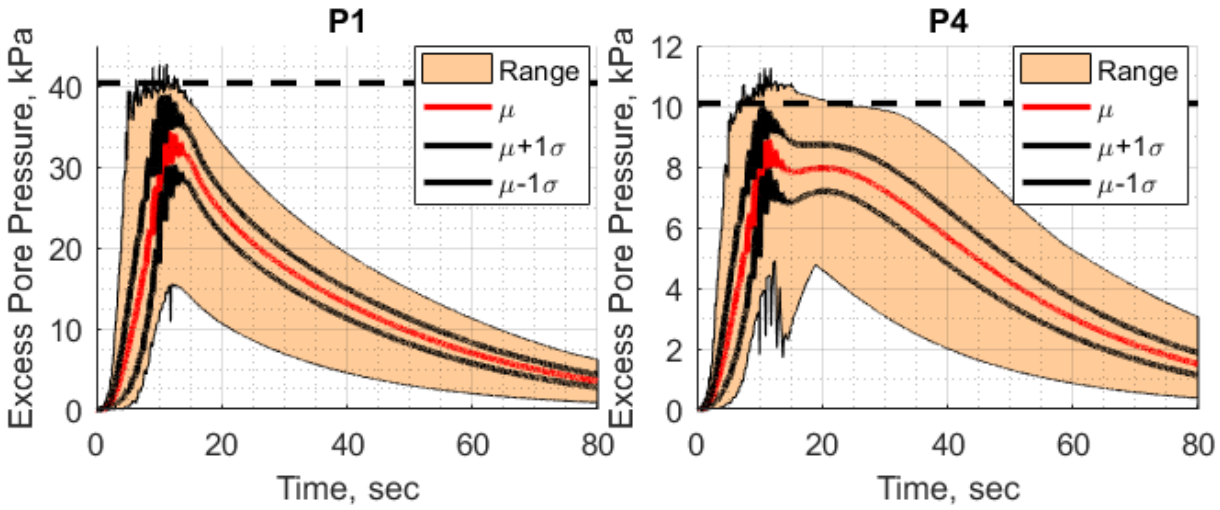

Figure 44: Excess pore pressure ratio for spatial variability case

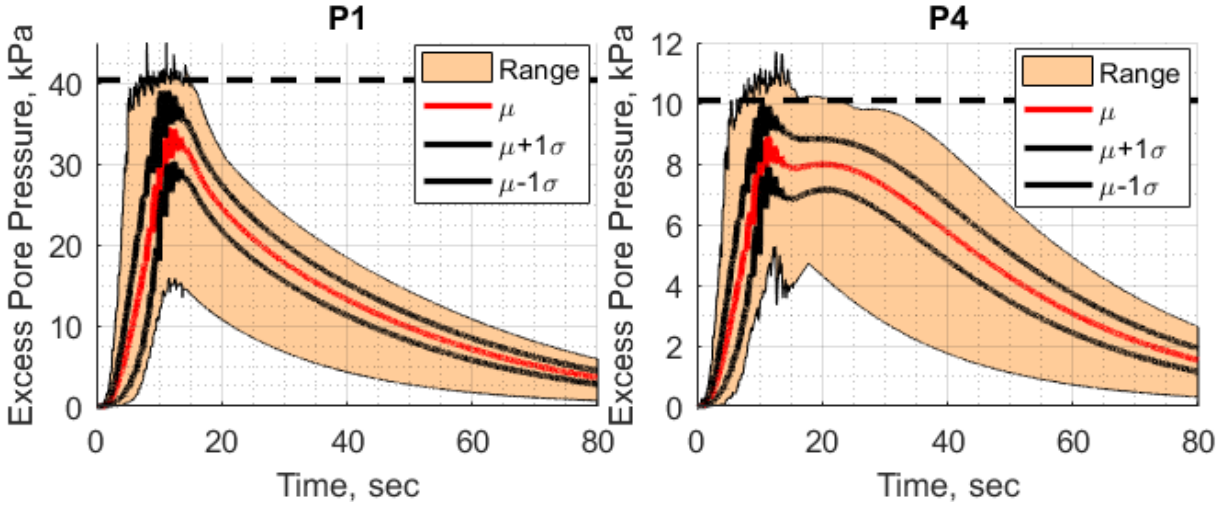

Figure 45: Excess pore pressure ratio for spatial and mean void ratio variability case

5.1.2. Soil Surface Response

Figure 46 shows the spread of lateral displacement time histories on the ground surface right above the central array of pore pressure sensors (Figure 1), as well as the time histories of the soil settlement on the ground surface right above the left array of pore pressure sensors. In this figure, the mean, mean +/- one standard deviation and range of displacements for the homogenous case are presented. In a similar fashion, Figure 47 shows the lateral and vertical displacements for the spatial variability case, while Figure 48 shows the results obtained by considering the spatial and mean void ratio variability.

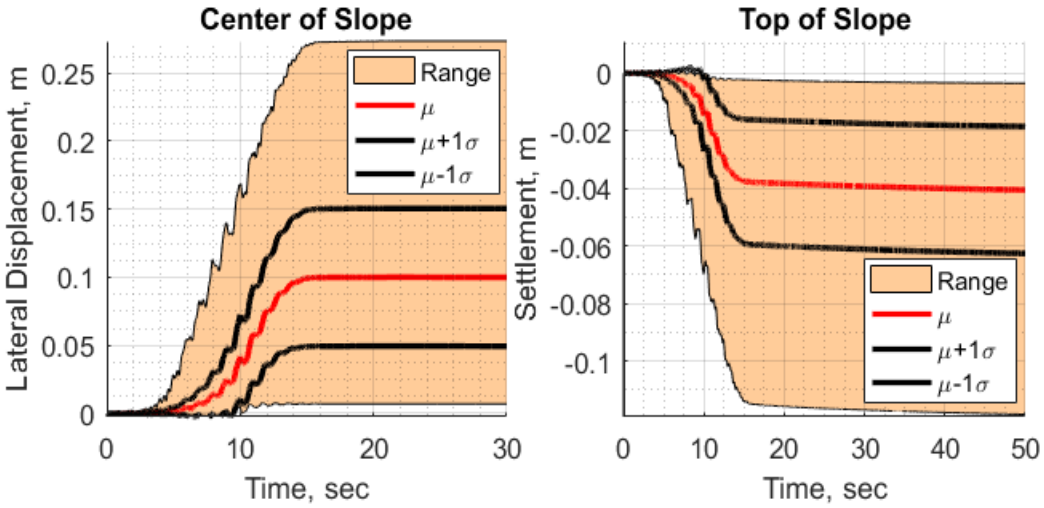

Figure 46: Time History of Displacement for Homogeneous Case

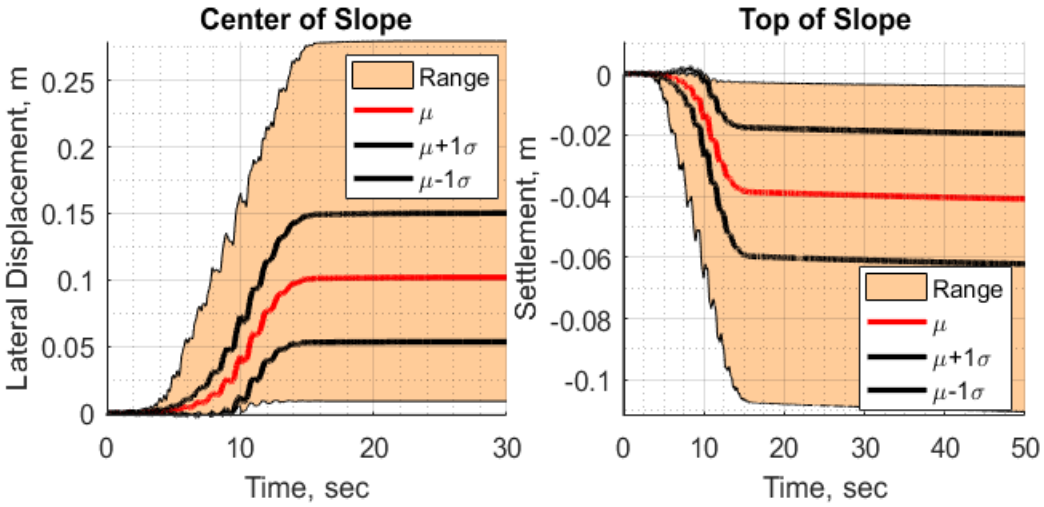

Figure 47: Time History of Displacement for Spatial Variability Case

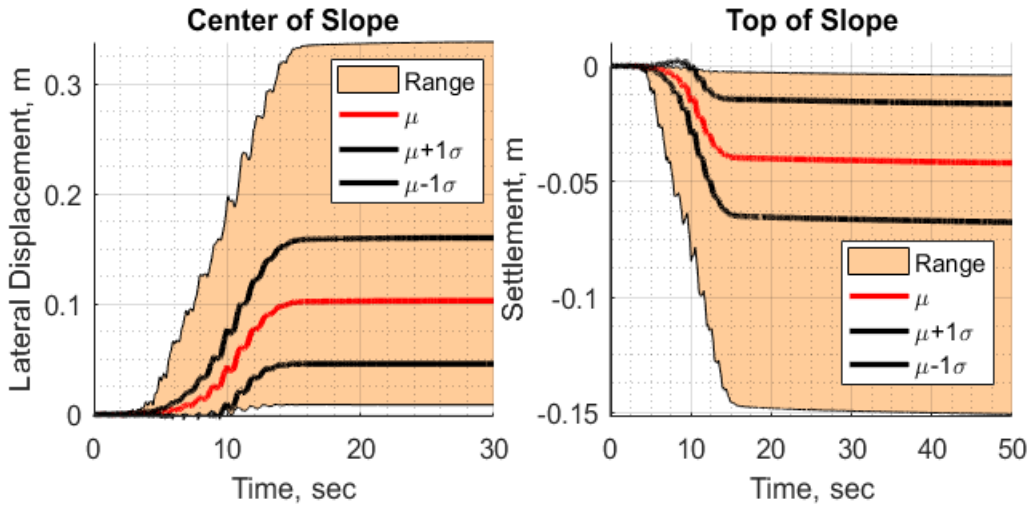

Figure 48: Time History of Displacement for Spatial and Mean Void Ratio Variability Case

5.1.3. Lateral Spreading Soil Profile

The variations of the lateral displacement profile at the central portion of the soil specimen (where P1 to P4 sensors are located) for the homogeneous, spatially variable cases as well as the case considering the spatial and mean variability are shown in Figure 49.

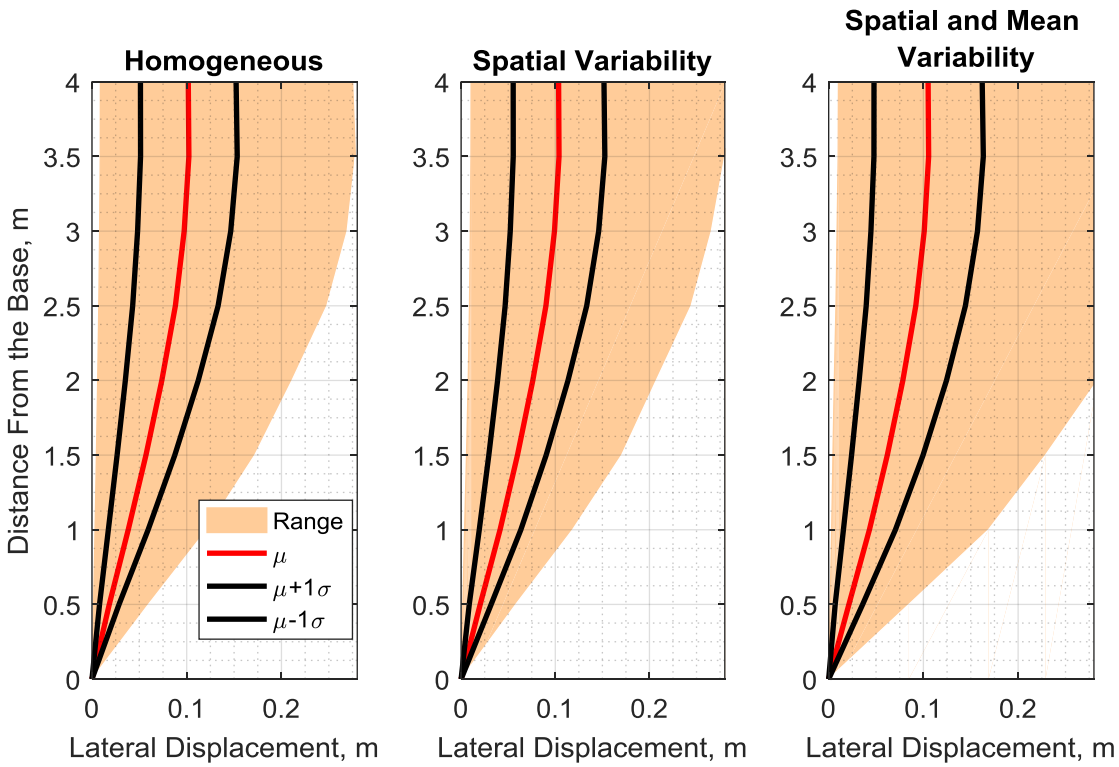

Figure 49: Soil profile lateral displacement at the center of the soil

5.1.4. Discussion

The results obtained from the MC simulations provide the following observations. First, a wide range of variation is observed in the generated excess pore pressures. The maximum excess pore pressure ratio ranged from 0.32 to 1.0 for the location of the pore pressure transducer P1 in the homogeneous case (Figure 43). For the location of P4, the range was from 0.45 to 1.0. A similar range can be seen in the spatial variability cases (Figures 44 and 45). While the average rate of excess pore pressure generation is similar for the homogeneous and spatial variability cases, a slightly higher peak is observed in the spatial variability case. Additionally, the range of variation of the rate of excess pore pressure dissipation is wider in the spatial variability cases. Figures 46 to 48 show the lateral displacement and settlement results at two different locations on the soil surface. In Figure 46, it can be seen that the soil response has a mean value of 10 and 4.05 cm for the lateral displacement and settlement of the homogenous case, respectively. While the coefficient of variation for the lateral displacement and settlement are 50.6 and 54.7%, respectively. For the spatial variability case the lateral displacement has a mean of 10.18 cm and coefficient of variation of 47.5% and the settlement has a mean of 4.07 cm and a coefficient of variation of 52.3%. Finally

the spatial and mean variability case show a mean lateral displacement of 10.33 cm with a coefficient of variation of 55.4% and a mean settlement of 4.19 cm with a coefficient of variation of 61.1%.

While the differences are small, it can be seen that smaller deformations are observed for the spatial variability case in both the mean and range of variation. Ultimately, it appears that the soil response is more sensitive to the base motion variability than to the spatial variability under the assumed conditions. This agrees with the observations made by Lopez-Caballero and Modaressi-Farahmand-Razavi [37]. Similar observations can be obtained from the results shown in Figure of the soil profile lateral displacement. A small difference between the mean response and coefficient of variation of the lateral displacements between the homogeneous and spatial variability cases is observed.

With such large range of variability in the computed soil displacements, it may be argued that the same level of uncertainty is present in the simplified methods used for lateral spreading estimation [53–55]. However, the types of uncertainty influencing the results of the two different analysis methods are quite different. The uncertainty present in the simplified method is an epistemic uncertainty that is based on the lack of information. On the other hand, the uncertainty studied here is the aleatory uncertainty that is based on the inherent variability of the soil.

5.1.5. Lateral Spreading, Penetration Resistance and Base Motion Intensity Correlation

The correlation between the magnitude of the soil lateral spreading and the soil penetration resistance (representing the soil density) and the base motion intensity is evaluated here. The peak ground acceleration (PGA), the cumulative average velocity (CAV5) and the arias intensity (Ia) are the three different intensity measures considered in this evaluation. Figures 50 to 52 compare the lateral spreading magnitudes obtained from the stochastic analysis in terms of the soil penetration resistance at the depth of 2 meters q_c (z=2.0m) and selected measures of the base motion intensity, i.e. PGA, CAV5 and Arias intensity (I_a). It is noted that qc2 is measured in each centrifuge tests by using a miniaturized cone penetrometer (Kutter et al, 2020). The simulation results presented here were obtained from the stochastic analysis case investigating the effects of the base motion variability and the spatial and average void ratio variability. A best-fit surface trend was obtained for the data. The equation representing the best fit surface is shown along with the coefficient of determination for each case. From this trend, it is clear that the Arias intensity provides a reasonable representation of the base motion intensity as opposed to the PGA. The CAV is also significantly better representative of the base motion intensity than the GPA (Fig. 51).

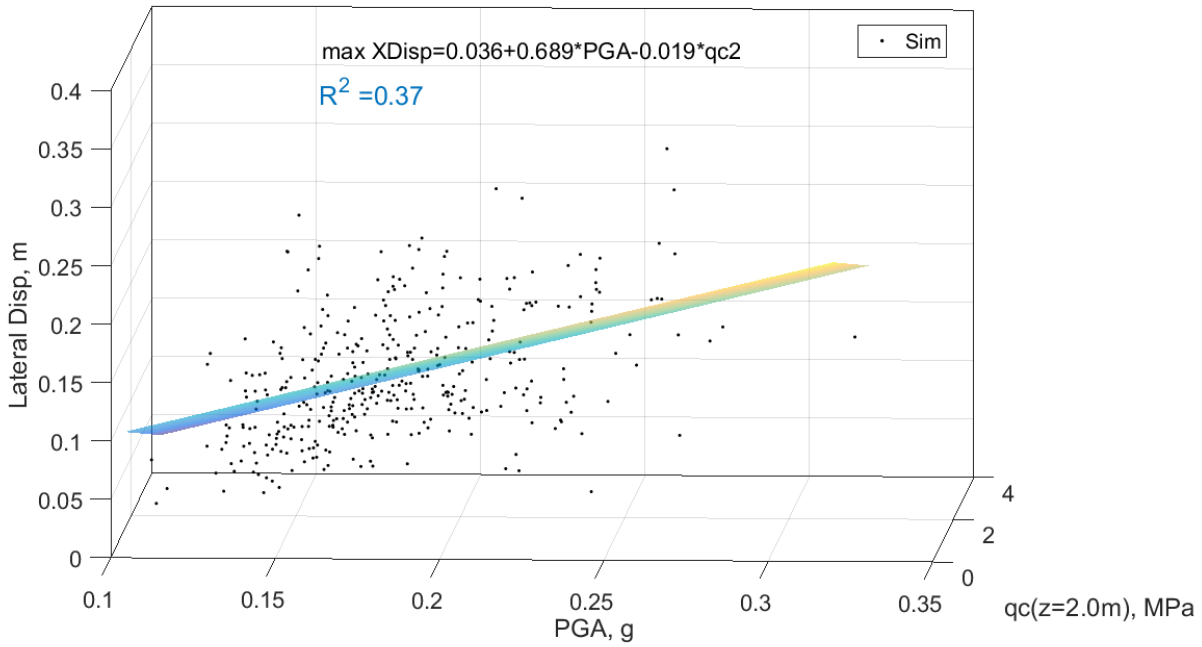

Figure 50: Correlation between Lateral Displacement, Penetration Resistance and PGA

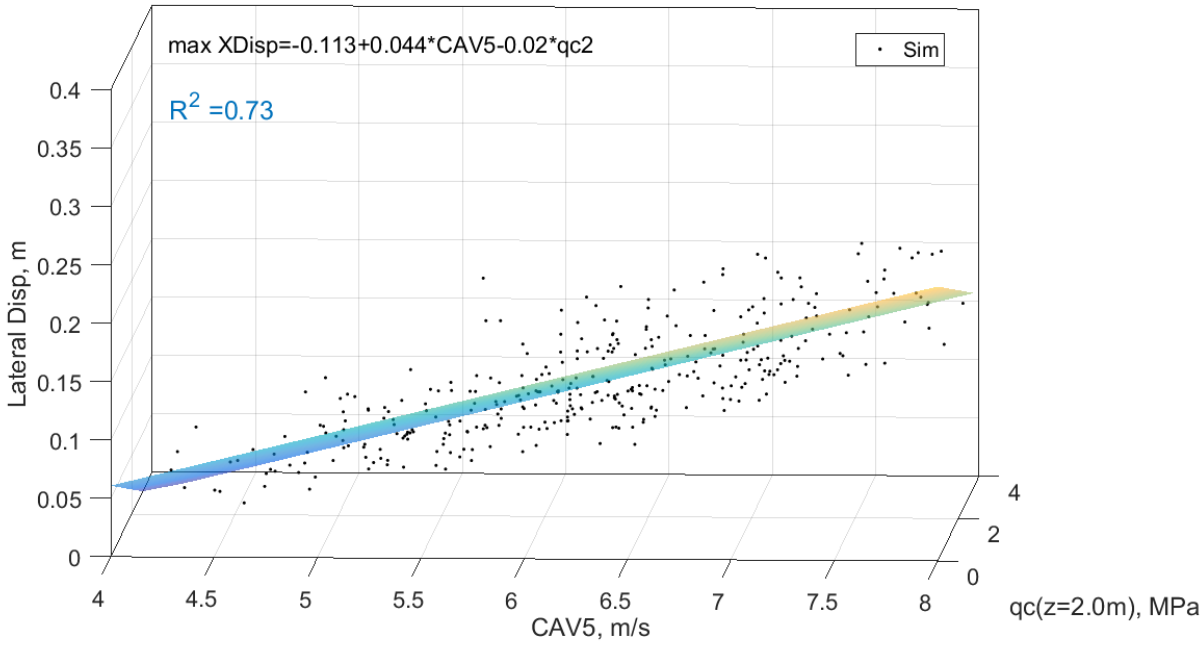

Figure 51: Correlation between Lateral Displacement, Penetration Resistance and CAV5

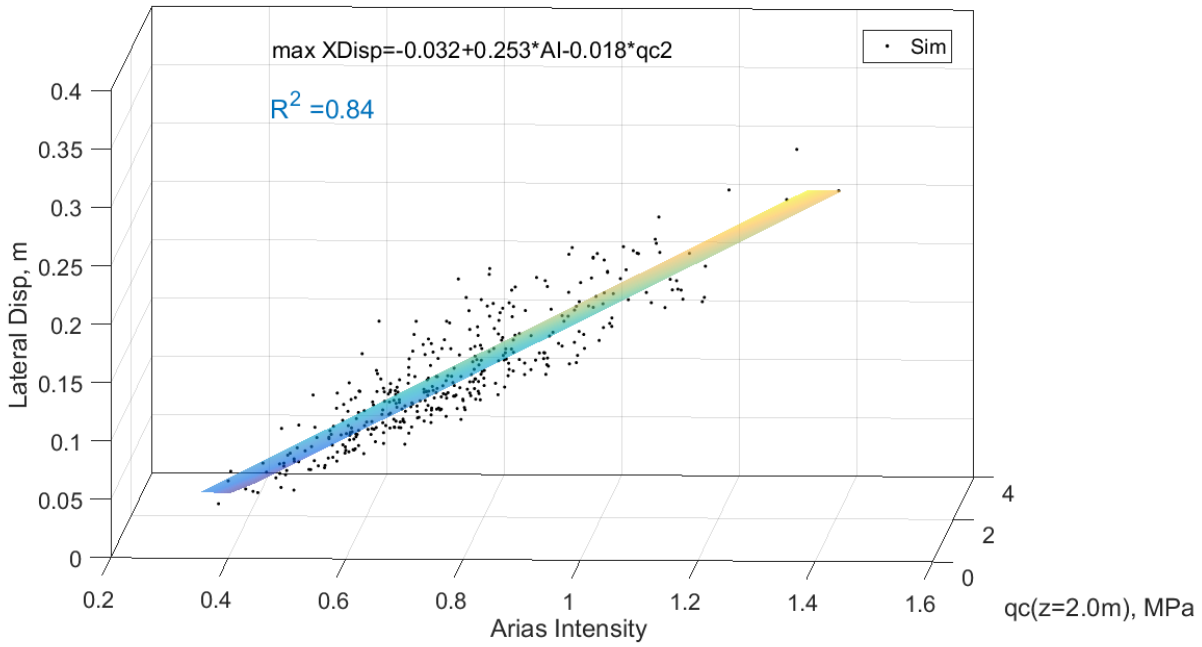

Figure 52: Correlation between Lateral Displacement, Penetration Resistance and Arias Intensity

5.1.6. Discussion

Figure 53 shows the joint probability density of the peak ground acceleration and the maximum excess pore pressure ratio. These results correspond to the maximum excess pore water pressure at the location of pore pressure transducer P1 for the homogeneous MC simulations. It can be seen that the joint probability density reaches a peak at maximum excess pore pressure ratio of 0.94 and a peak ground acceleration (PGA) of 0.177 g for the homogeneous case. The peak densities at two additional PGA magnitudes are also shown in the figure.

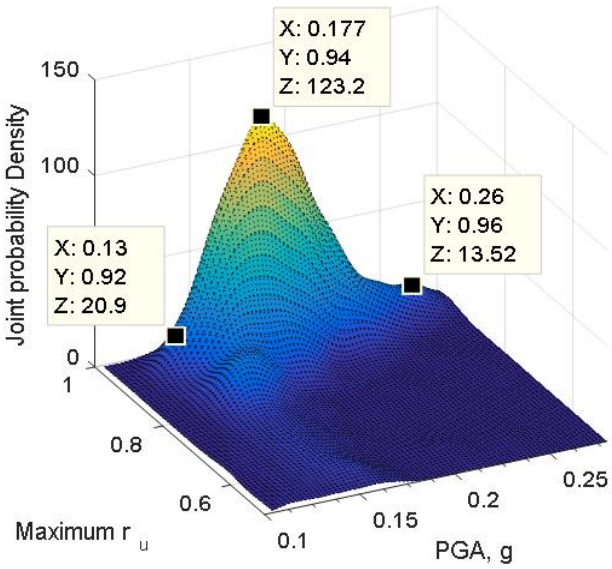

Figure 53: Joint probability density of PGA and maximum excess pore pressure

It is clear that the choice of the appropriate intensity measure can affect the correlation between the soil response and the base motion intensity. The PGA, as the peak value of the base motion time history, does not include sufficient information of the base motion characteristics and does not correlate well with the maximum excess pore pressure and lateral displacements developed in the sloping ground. The Arias intensity, on the other hand, is a more reasonable representation of the base motion characteristics and shows a better correlation with the maximum excess pore pressure and lateral displacements in the soil.

6. Comparison with Observed Variability in LEAP Experimental Results

In this section, the variability in the lateral spreading obtained from the stochastic analysis is compared to the variability observed in the centrifuge experiments performed during the LEAP-UCD-2017 project. The previously conducted analyses were performed by using assumed values obtained before the completion of the centrifuge testing for LEAP-UCD-2017. In order to have a proper comparison a more careful consideration of the assumed values is necessary. Therefore an additional set of simulations was performed. Previously, the variability in the soil density was considered based on the assumption that the mean density was 1.650 Mg/m^3 and a COV corresponding to the observed of +/- 100 kg/m^3. Here, the mean and coefficient of variation are assumed based on the reported test densities for the LEAP-UCD-2017 that are 1.651 Mg/m^3 and 1.82%, respectively.

While the previous simulations considered only the base motions with a target PGA of 0.15 g, the full suite of base motions obtained from LEAP-UCD-2017 is used in generating the synthetic base motion realizations in this simulation. Figure 54 shows the distribution of the response spectra of the base motions achieved in the LEAP-UCD-2017 centrifuge experiments. Figure 55 shows the distribution of the response spectra of the synthetic base motions generated for this study. The new set of realizations were generated in a fashion similar to the previous analyses. The figure shows how the mean and the mean +/- one standard deviation compare with what was observed in the centrifuge experiments.

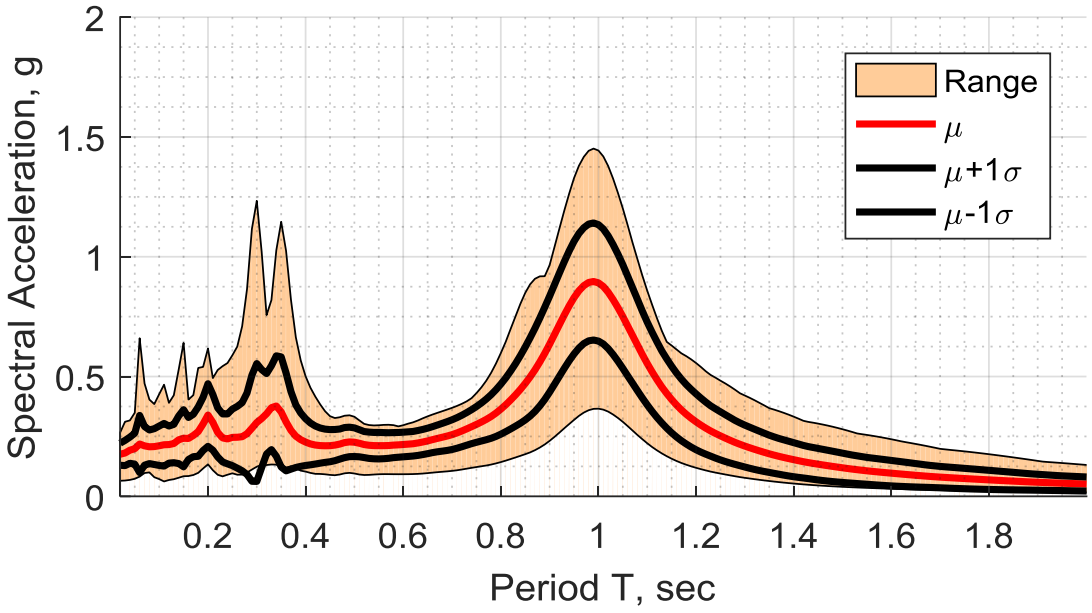

Figure 54: Distribution of the response spectra for the LEAP-UCD-2017 achieved base motions

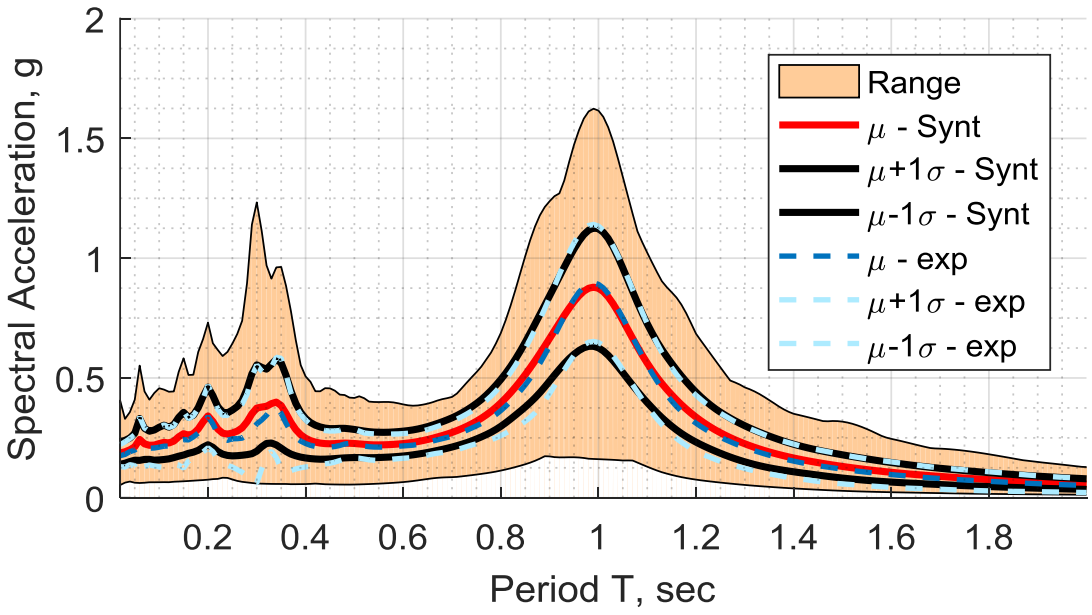

Figure 55: Distribution of the response spectra of generated synthetic base motion

In this study, a finer mesh was considered for the finite element model of the soil layer. This was considered to reduce the effects of the numerical error that may contribute to the variability of the results. Figure 56 shows a contour plot of the distribution of the initial void ratio of a single realization over the finite element mesh used in this study.

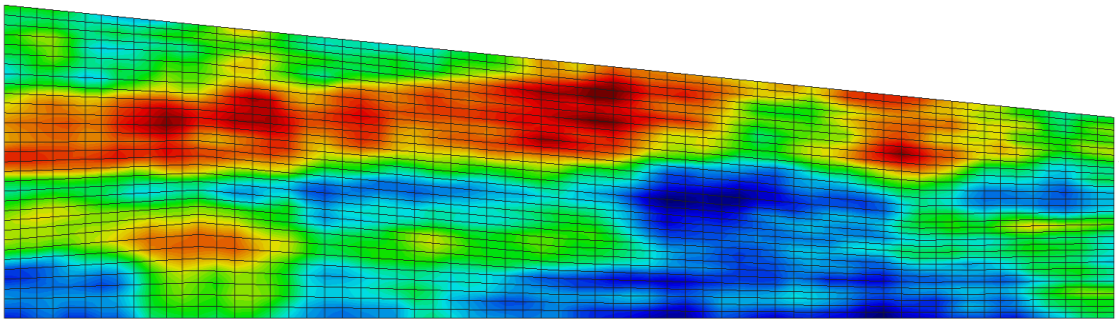

Figure 56: Distribution of Initial Void Ratio of a Single Realization

6.1.1. Excess Pore Pressure

Figure 57 shows the distribution of the excess pore pressure time history. The results are presented in the same manner as before, where the range, mean and mean +/- one standard deviation are plotted at the locations of pore pressure transducers P1 and P4. It can be seen that the larger range of variation in the base motions resulted in a much larger range of variation in the generated excess pore pressure.

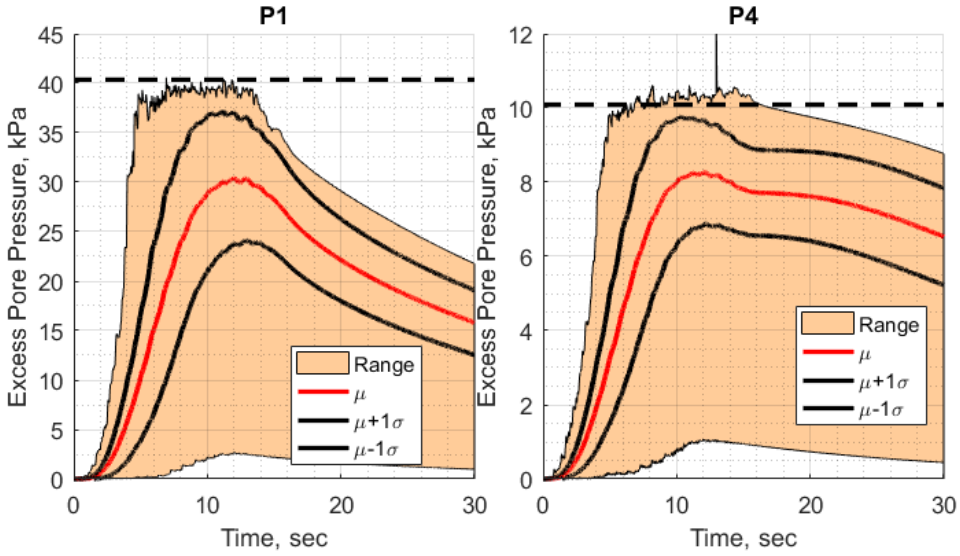

Figure 57: Excess Pore Pressure Distribution

6.1.2. Soil Surface Response

Figure 58 shows a plot of the time history of the lateral displacement at the center of the slope and the settlement at the top of the slope. The results show a mean lateral displacement of 13.5 cm with a COV of 59% and a mean settlement of 5.3 cm with a COV of 67%. It is important to note that the LEAP experiment reported a lateral displacement with a median of 13.3 cm, a mean of 18.1 cm and a COV of 66.4%.

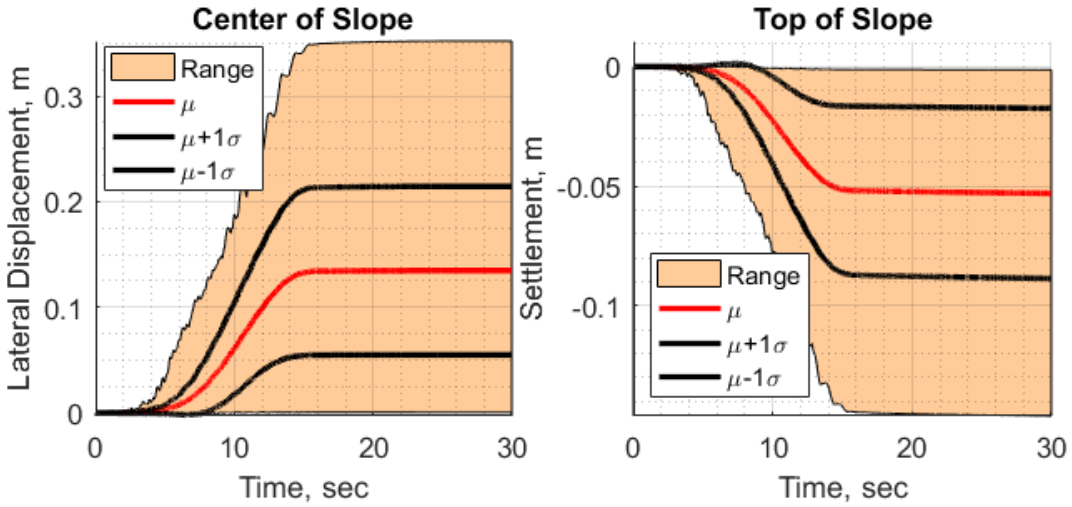

Figure 58: Time History of Displacement

6.1.3. Comparison of the stochastic analyses with experiment variabilities

The results obtained from the stochastic analysis are compared to the lateral displacements obtained from the centrifuge experiments. In order to properly compare the two sets of results, it is more appropriate to compare the results with respect to the achieved soil density and the magnitude of the achieved base motion. As it was shown in the previous section, presenting the results in terms of a soil penetration resistance at depth of 2 meters and the Arias intensity provides a better trend for correlating the soil density and magnitude of the base motion to the resulting displacement. In a similar fashion, the results obtained from this stochastic analysis and the LEAP centrifuge experiments are plotted in Figure 59. The 3D plot in this figure shows the variation of the measured and simulated lateral displacements in terms of the q_{c2} (MPa) and the arias intensity I_a (m/sec). The simulation results are plotted with black dots. A best-fit surface was obtained for the simulation data. The surface is a cubic polynomial and its coefficient of determination (r^2) is 0.85. The measured lateral displacement of each centrifuge experiment is shown with a distinct marker. The LEAP-UCD-2017 results are plotted with red markers. Additional tests were performed later for the LEAP-Asia 2019. These new results are

shown with blue markers. Figure 60 shows the same results in 2D plots.

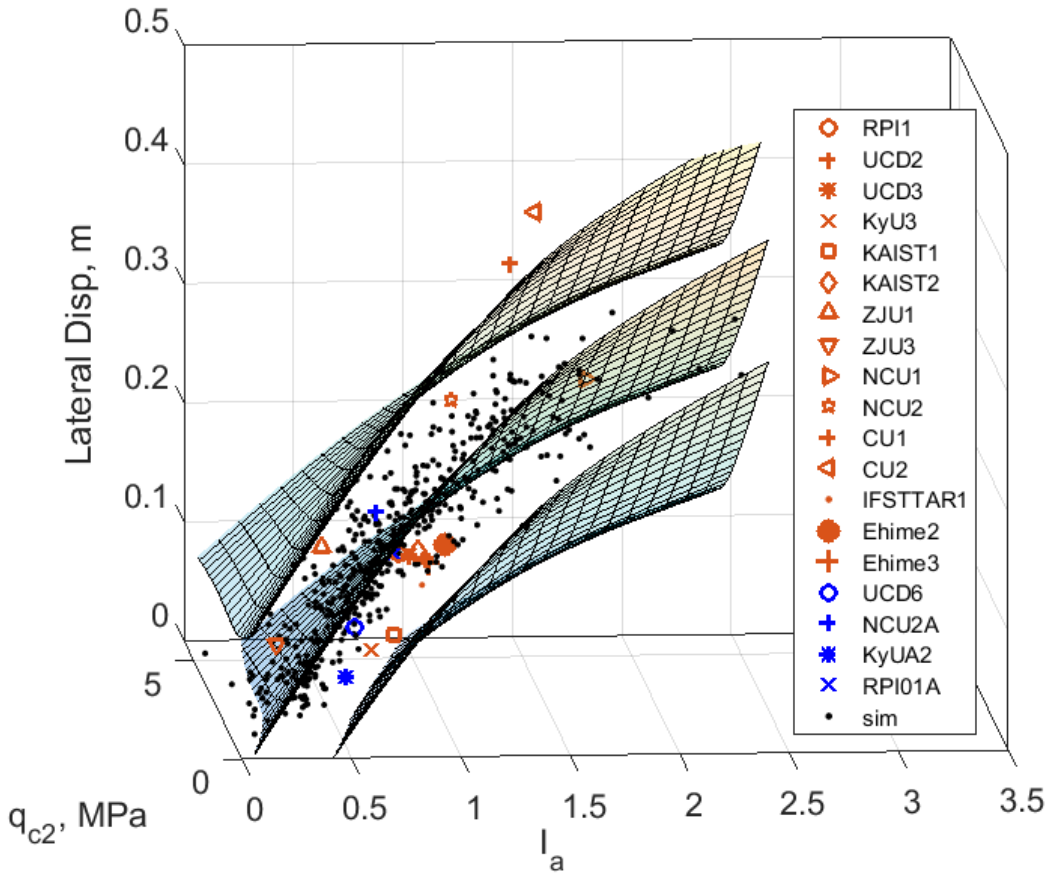

Figure 61 shows where the experimental data fall with respect to the bounds of the stochastic analysis. It can be seen that the variability observed in the stochastic simulations reasonably captures the variability observed in the experiments. Except for the centrifuge experiments performed at Cambridge University (CU1 and CU2), the simulation results envelop the experimental results.

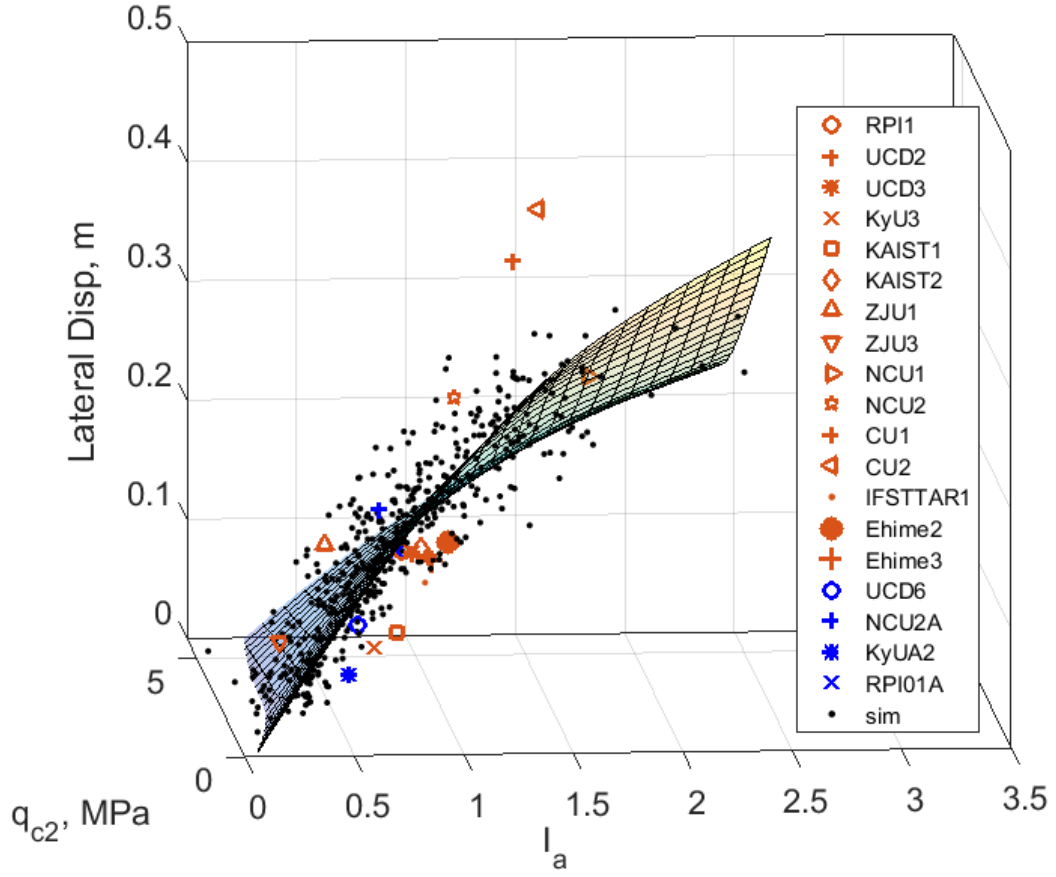

Figure 59: Comparison of the stochastic analysis results with the centrifuge experiments

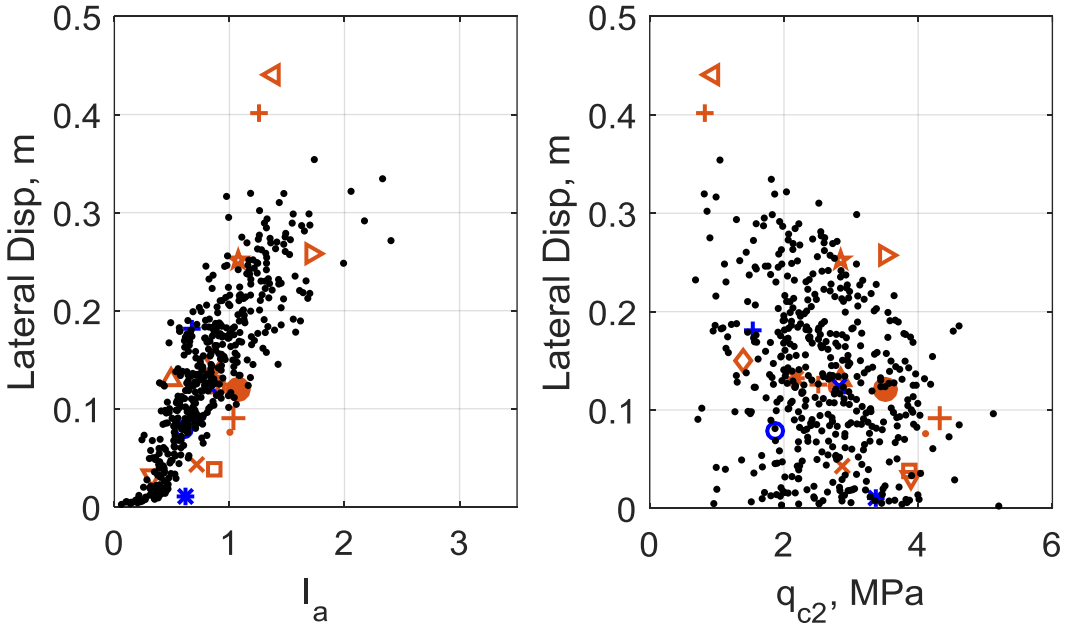

Figure 60: Lateral displacement versus arias intensity and penetration resistance in 2D

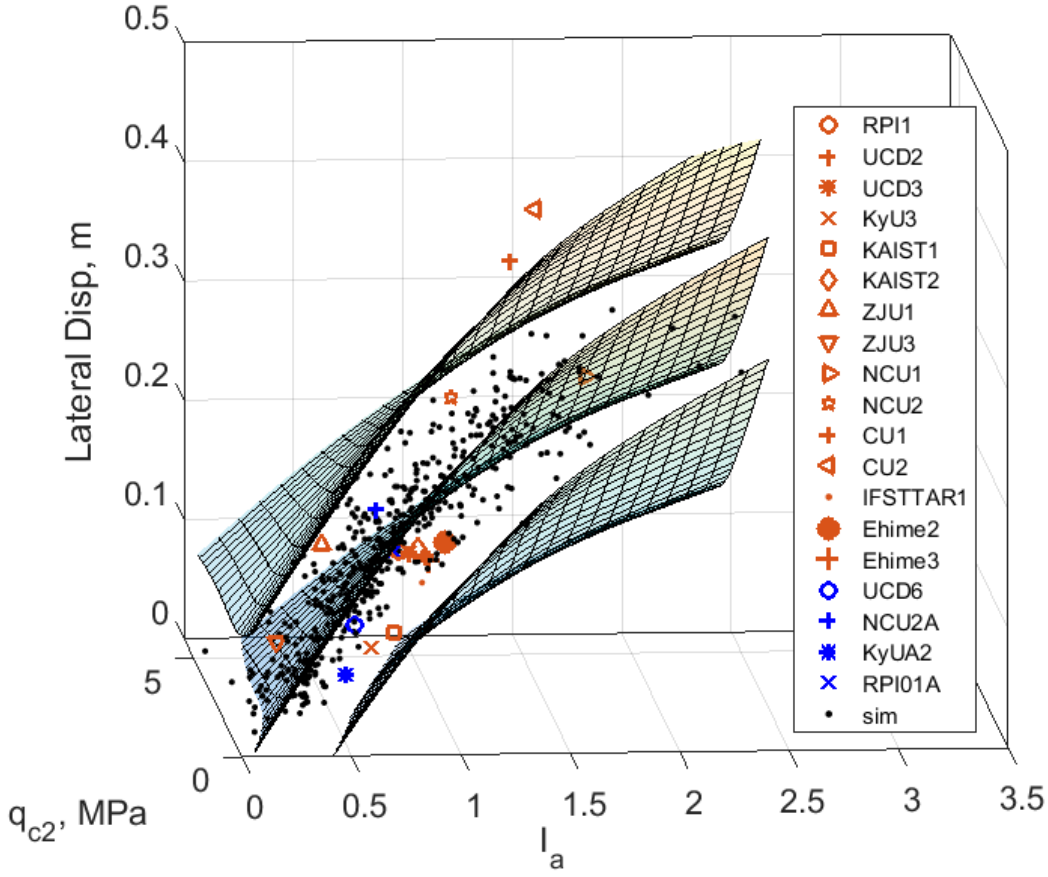

Figure 61: Comparison of the centrifuge experiments with the bounds of the stochastic analysis

7. Concluding Remarks:

The effects of two sources of variability on the lateral spreading of soil were investigated. The first source is the inherent spatial variability of the soil density and the second source is the variability in the magnitude and frequency of the base motion. The study was conducted using the random finite element method, where nonlinear finite element analysis coupled with Monte Carlos simulation is used. The soil behavior was modeled using a critical state soil plasticity model, which allows for modeling the spatial random fields independent of the model calibration. The variability in the base motion was modeled by generating synthetic acceleration time histories to match the distribution of the base motion response spectra achieved during LEAP-UCD-2017 project.

First, the effects of small variability of soil density on the response of liquefiable sloping ground were investigated. By considering the initial void ratio as a random variable with a normal distribution, a series of stochastic analyses were performed. The first case investigates the effects of epistemic variability of the initial void ratio caused by the inability to achieve the target density. The remaining cases investigate the effects of the spatial variability in the initial void ratio due to

the soil inherent heterogeneity and imperfections in specimen preparations. These cases demonstrate the effects of the presence of a trend in the definition of the mean, the effects of spatial correlation and the effects of the presence of a global constraint such as a specific average model density.

The results show that while the average excess pore pressure response is similar for all the five cases, the variations in the rate of excess pore pressure generation, maximum excess pore pressure and the rate of dissipation are different. The lateral displacements and surface settlements show a degree of variation that is dependent on how the random field is defined. The observed variability in the response would constitute the error in the results obtained from a uniformly modeled soil analysis. Therefore, in the cases where the variability is significant, the validity of the simulation may be compromised. The results showed that the variation in displacement is highly influenced by the average density of the centrifuge specimen. It was also shown that the lateral displacements and settlements can be modeled using normal as well as log-normal distributions, with the log-normal distribution proving to be more representative based on the goodness of fit test. Finally, the lateral displacements of the soil profile for the spatial variability cases were compared to the responses of different soil specimens prepared with uniform initial void ratios corresponding to various percentiles of the target distribution. It was shown that depending on the source of variability, the average response of the soil profile may correspond to that of a soil denser than the target density.

The variability in the achieved base motions of LEAP-2015 and LEAP-UCD-2017 centrifuge experiments was modeled as a random process and two cases of Monte Carlo simulations were performed to study the effects of this variability on the response of soil specimen in a homogeneous and a spatially variable conditions. The analysis results revealed a significant variation in the generated excess pore pressures and displacements due to the variability in the base motion. A coefficient of variation of about 50% in the soil deformations emphasizes the high level of sensitivity of the response of the liquefiable soil to variations in the input motions. On the contrary, a very small difference in the response is observed between the homogeneous case and spatial variability case. Moreover, a Monte Carlo simulation was performed to model the combined effect of mean and spatial variability in the soil density along with the variability in the base motion. Similar observations were obtained from this case.

Finally, the variability observed in the LEAP-UCD-2017 experiment was modeled using the same modeling technique used in the previous stochastic analyses. The corresponding mean and coefficient of variation of the soil density as well as the complete suite of achieved base motions were used in the latter analyses. The variability obtained from the simulation was compared to the observed variability in the results of the centrifuge experiments. It was shown that with proper modeling of the variability in the soil density and base motion excitations, the stochastic analysis could reasonably predict the variability observed in the experiment.

8. Acknowledgment:

The support from the US National Science Foundation through grants to the George Washington University, University of California, Davis, and Rensselaer Polytechnic Institute (CMMI 1635524, CMMI 1635307 and CMMI 1635040) is gratefully acknowledged.

9. References:

[1] Lumb P. The Variability of Natural Soils. Can Geotech J 1966;3:74–97. https://doi.org/10.1139/t66-009.

[2] Lacasse S, Nadim F. Uncertainties in Characterising Soil Properties. In: C. D. Shackleford, Nelson PP, Roth MJS, editors. Uncertain. Geol. Environ. From theory Pract., ASCE SSP 58, New York; 1996, p. 49–75.

[3] Jones A, Kramer S, Arduino P. Estimation of Uncertainty in Geotechnical Properties for Performance-Based Earthquake Engineering. Peer Rep 2002;16.

[4] Raychowdhury P. Effect of soil parameter uncertainty on seismic demand of low-rise steel buildings on dense silty sand. Soil Dyn Earthq Eng 2009;29:1367–78. https://doi.org/10.1016/j.soildyn.2009.03.004.

[5] Kasama K, Whittle AJ. Effect of spatial variability on the slope stability using Random Field Numerical Limit Analyses. Georisk Assess Manag Risk Eng Syst Geohazards 2016;10:42–54. https://doi.org/10.1080/17499518.2015.1077973.

[6] Lacasse S, Nadim F. Probabilistic geotechnical analyses for offshore facilities. Georisk Assess Manag Risk Eng Syst Geohazards 2007;1:21–42. https://doi.org/10.1080/17499510701204224.

[7] Vanmarcke EH. Random fields: Analysis and Synthesis. Cambridge, MA: MIT Press; 1983.

[8] Huber M. Soil variability and its consequences in geotechnical engineering. 2013.

[9] DeGroot DJ, Baecher GB. Estimating Autocovariance of In-Situ Soil Properties. J Geotech Eng 1993;119:147–66. https://doi.org/10.1061/(ASCE)0733-9410(1993)119:1(147).

[10] Campbell KW, Bozorgnia Y. Campbell-Bozorgnia NGA Ground Motion Relations for the Geometric Mean Horizontal Component of Peak and Spectral Ground Motion Parameters 2007:1–265.

[11] Campbell KW, Bozorgnia Y. NGA ground motion model for the geometric mean horizontal component of PGA, PGV, PGD and 5% damped linear elastic response spectra for periods ranging from 0.01 to 10 s. Earthq Spectra 2008;24:139–71. https://doi.org/10.1193/1.2857546.

[12] Kramer SL. Geotechnical Earthquake Engineering. Prentice Hall; 1996.

[13] Spanos PD, Vargas Loli LM. A statistical approach to generation of design spectrum compatible earthquake time histories. Int J Soil Dyn Earthq Eng 1985;4:2–8.

https://doi.org/10.1016/0261-7277(85)90029-4.

[14] Baker JW, Lee C. An Improved Algorithm for Selecting Ground Motions to Match a Conditional Spectrum. J Earthq Eng 2017:1–16. https://doi.org/10.1080/13632469.2016.1264334.

[15] Baker JW, Lin T, Shahi SK. New Ground Motion Selection Procedures and Selected Motions for the PEER Transportation Research Program - DRAFT. PEER Rep 2011;03:87.

[16] Jayaram N, Baker JW. Ground-Motion Selection for PEER Transportation Research Program. 7th Int Conf Urban Earthq Eng 5th Int Conf Earthq Eng 2010:9.

[17] Jayaram N, Lin T, Baker JW. A Computationally efficient ground-motion selection algorithm for matching a target response spectrum mean and variance. Earthq Spectra 2011;27:797–815. https://doi.org/10.1193/1.3608002.

[18] Rathje EM, Kottke AR, Trent WL. Influence of Input Motion and Site Property Variabilities on Seismic Site Response Analysis. J Geotech Geoenvironmental Eng 2010;136:607–19. https://doi.org/10.1061/(ASCE)GT.1943-5606.0000255.

[19] Gazetas G, Debchaudhury A, Gasparini D. Random vibration analysis for the seismic response of earth dams. Geotechnique 1981:261–77.

[20] Giaralis A, Spanos PD. Derivation of response spectrum compatible non-stationary stochastic processes relying on Monte Carlo-based peak factor estimation. Earthquakes Struct 2012;3:719–47. https://doi.org/10.12989/eas.2012.3.5.719.

[21] Preumont A. A method for the generation of artificial earthquake accelerograms. Nucl Eng Des 1980;59:357–68. https://doi.org/10.1016/0029-5493(80)90205-8.

[22] Vanmarcke, Erik H.; Gasparini D a. Simulated earthquake motions compatible with prescribed response spectra 1976:99.

[23] Beacher GB, Ingra TS. Stochastic FEM in Settlement Predictions. J Geotech Geoenvironmental Eng 1981;107:449–63.

[24] Vanmarcke E, Asce M, Grigoriu M. Stochastic Finite Element Analysis of Simple Beams 1984;109:1203–14.

[25] Sudret B, Der Kiureghian A. Comparison of finite element reliability methods. Probabilistic Eng Mech 2002;17:337–48. https://doi.org/10.1016/S0266-8920(02)00031-0.

[26] Stefanou G. The stochastic finite element method: Past, present and future. Comput Methods Appl Mech Eng 2009;198:1031–51. https://doi.org/10.1016/j.cma.2008.11.007.

[27] Fenton GA, Griffiths D V. Statistics of block conductivity through a simple bounded stochastic medium. Water Resour Res 1993;29:1825–30. https://doi.org/10.1029/93WR00412.

[28] Griffiths D V, Fenton G a. Seepage beneath water retaining structures founded on spatially random soil. Géotechnique 1993;43:577–87. https://doi.org/10.1680/geot.1993.43.4.577.

[29] Griffiths D V., Fenton GA. Probabilistic Settlement Analysis by Stochastic and Random Finite-Element Methods. J Geotech Geoenvironmental Eng 2009;135:1629–37. https://doi.org/10.1061/(ASCE)GT.1943-5606.0000126.

[30] Popescu R, Prevost JH, Deodatis G. Effects of spatial variability on soil liquefaction: some design recommendations. Géotechnique 1997;47:1019–36.

https://doi.org/10.1680/geot.1997.47.5.1019.

[31] Popescu R, Prevost JH, Deodatis G. 3D effects in seismic liquefaction of stochastically variable soil deposits. Géotechnique 2005;55:21–31.
https://doi.org/10.1680/geot.2005.55.1.21.

[32] Ural D. Liquefaction analysis: a probabilistic approach. Worl Conf Eathquake Eng 1996.

[33] Chakrabortty P, Popescu R, Phillips R. Liquefaction of heterogeneous sand: Centrifuge study. Geotech Test J 2011;34. https://doi.org/10.1520/GTJ102925.

[34] Popescu R. Effects of soil spatial variability on liquefaction resistance: Experimental and theoretical investigations. Deform Charact Geomaterials 2008:73–94.

[35] Montgomery J, Boulanger RW. Effects of Spatial Variability on Liquefaction-Induced Settlement and Lateral Spreading. J Geotech Geoenvironmental Eng 2017;143:04016086. https://doi.org/10.1061/(ASCE)GT.1943-5606.0001584.

[36] Boulanger RW, Montgomery J. Nonlinear deformation analyses of an embankment dam on a spatially variable liquefiable deposit. Soil Dyn Earthq Eng 2016;91:222–33. https://doi.org/10.1016/j.soildyn.2016.07.027.

[37] Lopez-Caballero F, Modaressi-Farahmand-Razavi A. Assessment of variability and uncertainties effects on the seismic response of a liquefiable soil profile. Soil Dyn Earthq Eng 2010;30:600–13. https://doi.org/10.1016/j.soildyn.2010.02.002.

[38] Kutter, B. L., Carey, T. J., Hashimoto, T., Zeghal, M., Abdoun, T., Kokkali, P., Madabhushi, G., Haigh, S. K., Burali d'Arezzo, F., Madabhushi, S., Hung, W. Y., Lee, C. J., Cheng, H. C., Iai, S., Tobita, T., Ashino, T., Ren, J., Zhou, Y. G., Chen, Y. M., Sun, Z. B., and Manzari, M. T. (2017). "LEAP-GWU-2015 experiment specifications, results, and comparisons." *Soil Dynamics and Earthquake Engineering*, 113, 616–628.
https://doi.org/10.1016/j.soildyn.2017.05.018

[39] Kutter, B. L., Carey, T. J., Stone, N., Zheng, B. L., Gavras, A., Manzari, M. T., Zeghal, M., Abdoun, T., Korre, E., Escof, S., Haigh, S. K., Madabhushi, G. S. P., Madabhushi, S. S. C., and Hung, W. (2020). *LEAP-UCD-2017 Comparison of Centrifuge Test Results*. *Model Tests and Numerical Simulations of Liquefaction and Lateral Spreading*, (B. L. Kutter, M. T. Manzari, and M. Zeghal, eds.), Springer International Publishing, Cham.

[40] Dafalias YF, Manzari MT. Simple Plasticity Sand Model Accounting for Fabric Change Effects. J Eng Mech 2004;130:622–34. https://doi.org/10.1061/(ASCE)0733-9399(2004)130:6(622).

[41] Manzari MT, Dafalias YF. A Critical State Two-Surface Plasticity Model for Sands. Geotechnique 1997;47:255–72.

[42] Vasko A. An Investigation into the Behavior of Ottawa Sand through Monotonic and Cyclic Shear Tests. George Washington University, 2015.

[43] Vasko A, ElGhoraiby MA, Manzari MT. LEAP-GWU-2015 Laboratory Tests. Dataset 2018. https://doi.org/10.17603/DS2TH7Q.

[44] Manzari, M. T., El Ghoraiby, M., Zeghal, M., Kutter, B. L., Arduino, P., Barrero, A. R., Bilotta, E., Chen, L., Chen, R., Chiaradonna, A., Elgamal, A., Fasano, G., Fukutake, K., Fuentes, W., Ghofrani, A., Haigh, S. K., Hung, W.-Y., Ichii, K., Kim, D. S., Kiriyama, T., Lascarro, C., Madabhushi, G. S. P., Mercado, V., Montgomery, J., Okamura, M., Ozutsumi, O., Qiu, Z., Taiebat, M., Tobita, T., Travasarou, T., Tsiaousi, D., Ueda, K., Ugalde, J., Wada, T., Wang, R., Yang, M., Zhang, J.-M., Zhou, Y.-G., and Ziotopoulou, K. (2020b). "LEAP-2017: Comparison of the Type-B Numerical Simulations with Centrifuge Test Results." *Model Tests and Numerical Simulations of Liquefaction and Lateral Spreading*, Springer International Publishing, Cham, 187–218.

[45] ElGhoraiby MA, Park H, Manzari MT. LEAP-2017 GWU Laboratory Tests 2018. https://doi.org/10.17603/DS2210X.

[46] ElGhoraiby M, Park H, Manzari MT. Physical and Mechanical Properties of Ottawa F65 Sand. In: Kutter B, Manzari M, Zeghal M, editors. Model Tests Numer. Simulations Liq. Lateral Spreading, Springer - In press; 2019, p. 41–62.

[47] ElGhoraiby M. Modeling of Liquefaction-Induced Lateral Spreading. George Washington University, 2019.

[48] Manzari, M. T., ElGhoraiby, M., Kutter, B. L., Zeghal, M., Abdoun, T., Arduino, P., Armstrong, R. J., Beaty, M., Carey, T., Chen, Y., Ghofrani, A., Gutierrez, D., Goswami, N., Haigh, S. K., Hung, W.-Y., Iai, S., Kokkali, P., Lee, C.-J., Madabhushi, S. P. G., Mejia, L., Sharp, M., Tobita, T., Ueda, K., Zhou, Y., and Ziotopoulou, K. (2017). "Liquefaction experiment and analysis projects (LEAP): Summary of observations from the planning phase." *Soil Dynamics and Earthquake Engineering,* 113, 714-743. https://doi.org/10.1016/j.soildyn.2017.05.015.

[49] Manzari, M. T., Ghoraiby, M. El, Zeghal, M., Kutter, B. L., Arduino, P., Barrero, A. R., Bilotta, E., Chen, L., Chen, R., Chiaradonna, A., Elgamal, A., Fasano, G., Fukutake, K., Fuentes, W., and Ghofrani, A. (2020a). *LEAP-2017 Simulation Exercise: Calibration of Constitutive Models and Simulation of the Element Tests*. *Model Tests and Numerical Simulations of Liquefaction and Lateral Spreading*, (B. L. Kutter, M. T. Manzari, and M. Zeghal, eds.), Springer International Publishing, Cham.

[50] Kokkali P, Abdoun T, Zeghal M. Physical modeling of soil liquefaction: Overview of LEAP production test 1 at Rensselaer Polytechnic Institute. Soil Dyn Earthq Eng 2017;113:629–49. https://doi.org/10.1016/j.soildyn.2017.01.036.

[51] Korre E, Abdoun T, Zeghal M. Verification of the Repeatability of Soil Liquefaction

Centrifuge Testing at Rensselaer. Model Tests Numer. Simulations Liq. Lateral Spreading, Cham: Springer International Publishing; 2020, p. 385–400. https://doi.org/10.1007/978-3-030-22818-7_19.

[52] Constantine PG, Wang Q. Random Field Simulation. Mathworks File Exch 2012. https://www.mathworks.com/matlabcentral/fileexchange/27613-random-field-simulation.

[53] Youd TL. Liquefaction-Induced Lateral Ground Displacement. 3rd Int. Conf. Recent Adv. Geotech. Earthq. Eng. Soil Dyn., 1995.

[54] Youd TL, Hansen CM, Bartlett SF. Revised multilinear regression equations for prediction of lateral spread displacement. J Geotech Geoenvironmental Eng 2002;128. https://doi.org/10.1061/(ASCE)1090-0241(2002)128:12(1007).

[55] Chu DB, Stewart JP, Youd TL, Chu BL. Liquefaction-Induced Lateral Spreading in Near-Fault Regions during the 1999 Chi-Chi, Taiwan Earthquake. J Geotech Geoenvironmental Eng 2006;132:1549–65. https://doi.org/10.1061/(ASCE)1090-0241(2006)132:12(1549).